

Earliest Triassic microbial mounds indicate an ‘oasis’ for recovery of life following the end-Permian extinction

Dan Qiao ^{a,b,c}, Zhiqiang Shi ^{a,d,*}, Jiangong Wang ^b, Kui Wu ^e, Shenyuan Peng ^{a,d}, Michael J. Benton ^f

^a Institute of Sedimentary Geology, Chengdu University of Technology, Chengdu 610059, China

^b Petrochina Northwest Research Institute of Petroleum Exploration & Development, Lanzhou 730020, China

^c College of Geological Science and Engineering, Shandong University of Science and Technology, Qingdao 266590, China

^d State Key Laboratory of Oil and Gas Reservoir Geology and Exploitation, Chengdu University of Technology, Chengdu 610059, China

^e Hubei Key Laboratory of Resources and Eco-environmental geology, Hubei Institute of Geosciences, Hubei Geological Bureau, Wuhan 430034, China

^f School of Earth Sciences, University of Bristol, Bristol BS8 1TQ, UK



ARTICLE INFO

Editor: H Falcon-Lang

Keywords:

Earliest Triassic
Microbial mound
Metazoan assemblages
Marine ecosystems
Upper Yangtze

ABSTRACT

Metazoan assemblages are rare in Early Triassic successions because of stressful environments in shallow seas after the end-Permian mass extinction (EPME). There is active debate about whether life in the oceans recovered rapidly or was delayed by up to 6–7 Myr. Here we present a new seabed assemblage showing evidence for relatively diverse animals in the middle Griesbachian, less than 1 Myr after the EPME crisis. The fossils are in microbial mounds from Chongqing, in the Upper Yangtze region, SW China, primarily composed of calcified filamentous cyanobacteria, including *Cyanonema*, *Rivulariaceae*, and *Girvanellaceae*, as well as planktonic calcareous microorganisms (calicispheres). The animals of the microbial mound include relatively common microconchids, sponges, gastropods and bivalves, and less abundant echinoderms and brachiopods. These metazoan communities differ among sub-facies of the microbial mound deposits, implying diverse ecosystem structures during the growth phase of the mounds. This kind of microbial mound might not only be typical of the aftermath of the mass extinction, but also have served as an ‘oasis’ for animals in the otherwise inhospitable environments of the Early Triassic seas.

1. Introduction

Microbialites are common structures in Early Triassic strata from shallow marine settings, and are often found at the Permian-Triassic boundary (PTB) (e.g. Kershaw et al., 2007; Mata and Bottjer, 2012; Woods, 2014; Wu et al., 2017; Zhang et al., 2020). At this time, microbial communities acted as disaster taxa that emerged after the end-Permian mass extinction (EPME) (Kershaw et al., 2011). Although PTB microbialites have been intensively studied in terms of their morphological structures (e.g. Tang et al., 2017; Kershaw et al., 2021), diagenetic processes (e.g. Friesenbichler et al., 2018), and ecological implications (e.g. Zhang et al., 2020), a lingering issue is how such benthic microbial communities developed during the Griesbachian (252.4–251.7 Ma) following the EPME. Stromatolites from the Elikah Formation in central Iran were the first described Lower Triassic (Griesbachian) microbialites, proposed as examples of anoxic or dysoxic

deposition by Wignall and Twitchett (2002). However, their microbial communities are rarely discussed.

Early Triassic benthic ecosystems were exposed to rigorous environments (Brayard et al., 2011). This reflects the fact that temperatures continued to be as high during the Early Triassic and earliest Middle Triassic as they had been at the PTB heat pulse, whether such high temperatures were sporadic (Sun et al., 2012) or continuous (Joachimski et al., 2012) through those 6–7 Myr. Certain animal groups may have recovered rapidly at points during the Early Triassic, but where later eliminated by the next heat pulse (Chen and Benton, 2012); this instability of Early Triassic marine faunas is confirmed by computational analysis of ecosystem stability (Guo et al., 2023).

The appearance of metazoan-dominated benthic ecosystems often serves as a marker for the late Early Triassic (Pisera, 1996; Pruss and Bottjer, 2004; Baud et al., 2008; Foster and Twitchett, 2014). Indeed, reports of earliest Early Triassic (Griesbachian) benthic ecosystems are

* Corresponding author at: Institute of Sedimentary Geology, Chengdu University of Technology, Chengdu 610059, China.

E-mail address: szqcdut@163.com (Z. Shi).

uncommon. Numerous studies have noted the change in quantitative fossil data of marine benthonic organisms from the end-Permian (Changhsingian) to the earliest Triassic (e. g. Chen et al., 2005; Brayard et al., 2006; Wu et al., 2018). A poor-quality, skeletonized marine fossil record has been documented from shallow facies within earliest Early Triassic sedimentary sequences (Brayard et al., 2011; Foster and Twitchett, 2014), suggesting that microbial-dominated benthic ecosystems prevailed at this time of severe environmental stress (Algeo et al., 2011; Xie et al., 2017). A diverse, very early Triassic (250.8 Ma) marine fauna was reported from South China (Dai et al., 2023).

Here, we report a remarkable early post-extinction animal fauna, found in Griesbachian microbial mounds from Baimiaozi-A (BMZ-A), Baimiaozi-B (BMZ-B) Tuanshanbao (TSB), and Yanjingxi (YJX) in Chongqing, Upper Yangtze region (Fig. 1). Our aim is to supplement the sparse record of earliest Triassic marine ecosystems in order to provide new insights into the initial recovery of marine benthic ecosystems after the EPME.

2. Stratigraphy and studied sections

The investigated sections are located on the Yangtze block within Chongqing city (Fig. 1), which was situated in the eastern part of the Paleo-Tethys Ocean, near the equator, during the Early Triassic. The fossils come from the earliest Triassic Feixianguan Formation, which is conformably underlain by the Changxing Formation and conformably overlain by the Jialingjiang Formation (Qiao et al., 2016). The

Feixianguan Formation is divided into four members in the Chongqing area based on outcrops and seismic-data analysis (e.g., Qiao et al., 2010; Wang et al., 2015; Zheng et al., 2023). The 1st (T_1f^1) and 2nd (T_1f^2) members were deposited in platform interiors (Qiao et al., 2010). The 3rd member (T_1f^3), the main gas pay reservoirs in Chongqing (Wang et al., 2015), consists of purple mudstone to grainstone, mainly deposited on the shallow platform margin (Zhang et al., 2012; Qiao et al., 2016). The 4th member (T_1f^4) is composed of purple-grey mudstone, anhydrite, and dolomite deposited in the tidal flats of the platform (Li et al., 2018).

Here, we study four outcrop sections that expose the 1st member of the Feixianguan Formation (carbonate platform facies), namely BMZ-A, BMZ-B, TSB, and YJX (Fig. 2). The BMZ-A and -B sections are mainly composed of marl, mudstone, ooid/intraclastic grainstone, and microbial mounds, and they have a refined chronostratigraphic framework (Duan et al., 2018). All four studied sections are very fossiliferous, mainly yielding microbial mats, small brachiopods, bivalves, conodonts, etc., with BMZ-B also yielding trace fossils. The BMZ-A and BMZ-B sections (Fig. 1C) are situated 1.5 km southeast of the Beibei district, Chongqing city and are located on both banks of the Jialing River, a branch of the upper reaches of the Yangtze River. At BMZ-A (Fig. 2), the *Isarcicella isarcica* conodont zone occurs from about 21 m to 37 m within the 1st member of the Feixianguan Formation (Duan et al., 2018), and suggests an earliest Triassic age (Griesbachian) (Jiang et al., 2010). The TSB section (Fig. 1D) is located 7 km northeast of the BMZ section (Fig. 1B) and is a newly surveyed section. Similar lithologies between

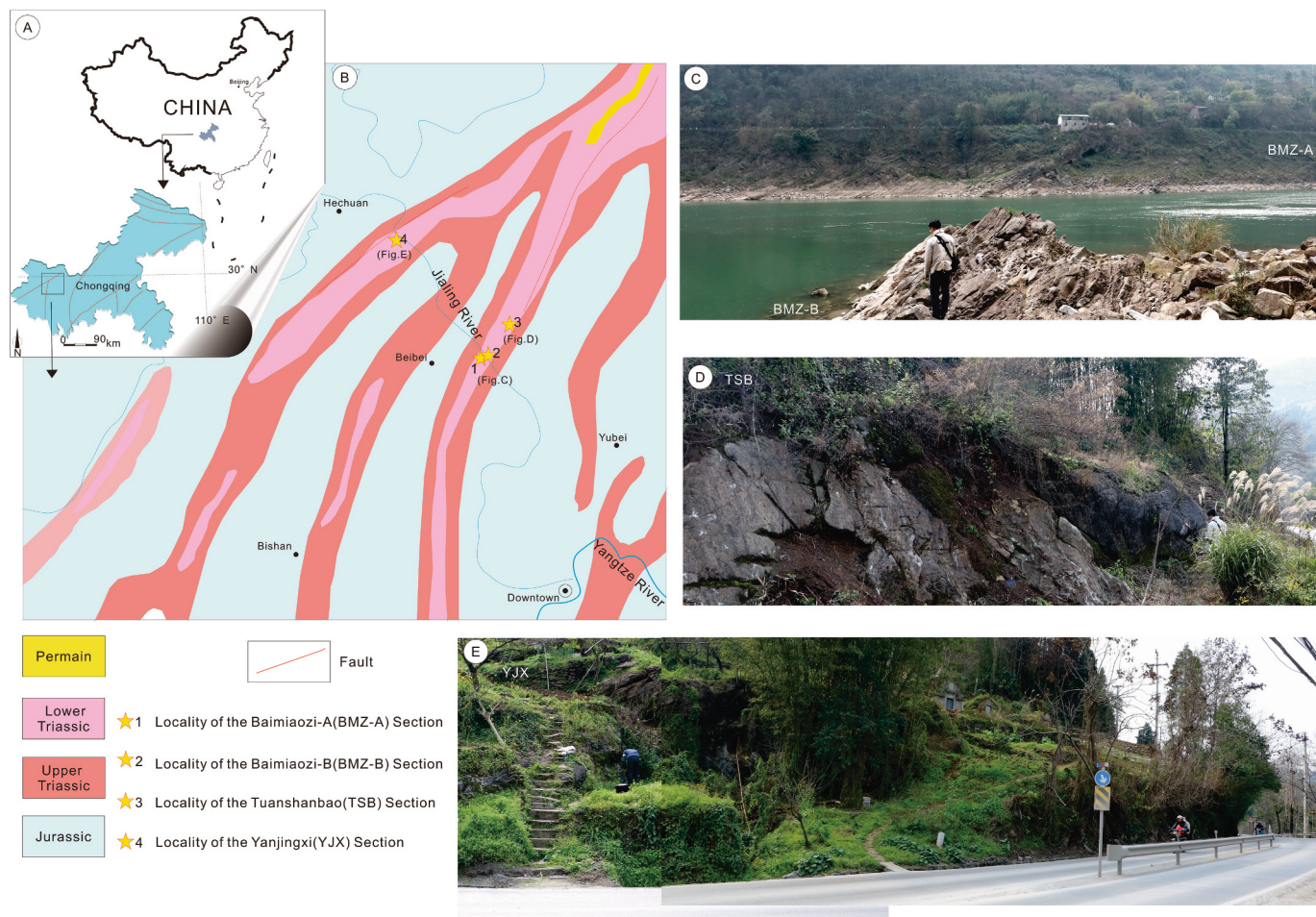


Fig. 1. Generalized geologic map of the study area showing the locations of the chosen stratigraphic sections. (A) Inset map of the People's Republic of China showing the location of the study area. (B) Geological map of the study area from Duan et al. (2018). (C) Overview of the BMZ section. (D) Overview of the TSB section. (E) Overview of the YJX section.

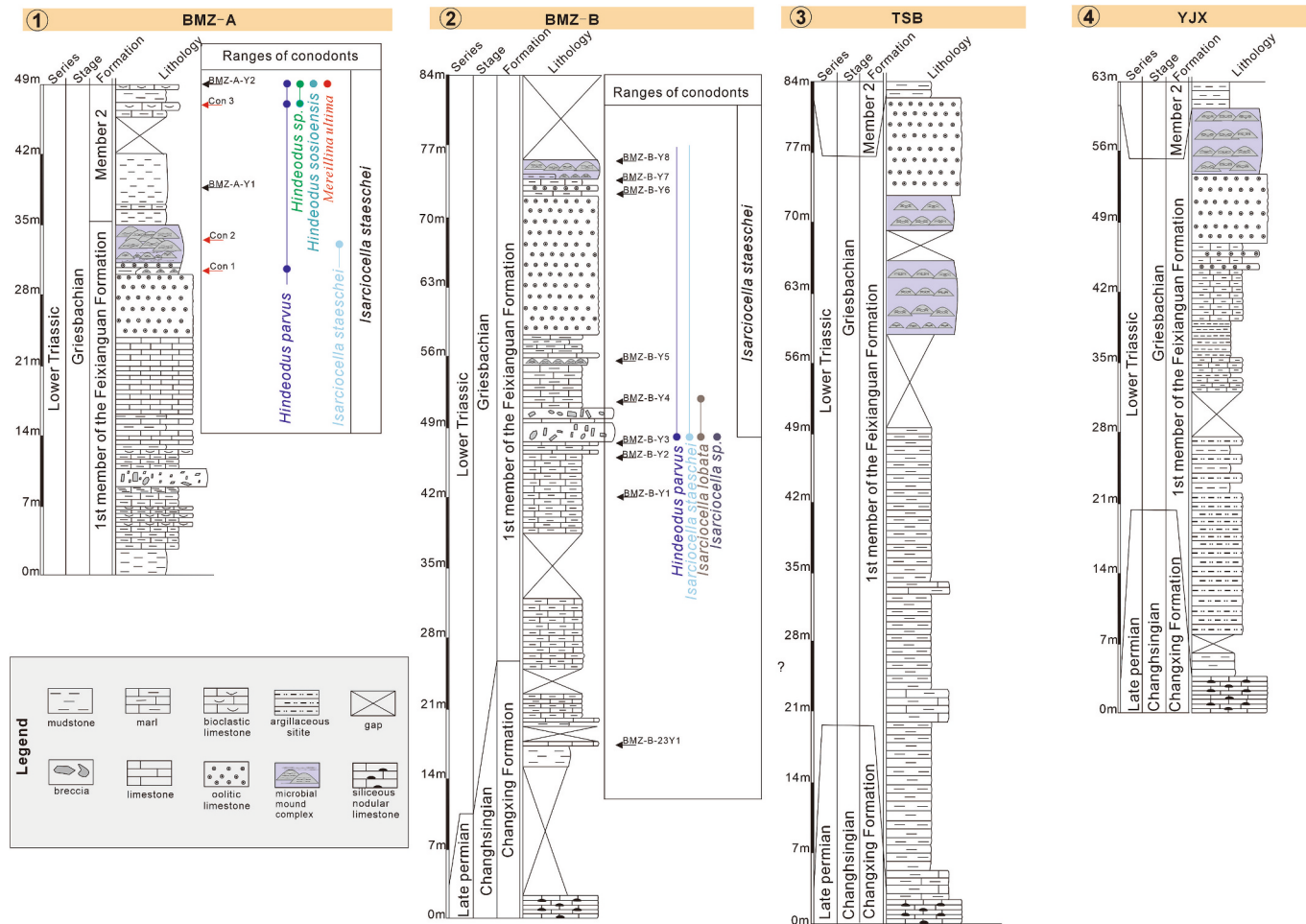


Fig. 2. Detailed sedimentological logs of 1st member of the Feixianguan Formation at the 4 study localities.

BMZ and TSB suggest that their chronostratigraphic frameworks should be approximately the same (Fig. 2). The YJX section, located about 30 km from the BMZ section, is situated in the Hechuan district, Chongqing city (Fig. 1B). Here, the Lower Triassic comprises the Feixianguan and Jialingjiang formations. The 1st Member of the Feixianguan Formation is marked by alternating layers of purple-yellow-green muddy limestone-dominated successions (Fig. 1E). In BMZ-B section, the lower strata of the microbial mound in 1st Member of the Feixianguan Formation consist, from bottom to top, of purple marl, grey grain limestone, and oolitic limestone (Fig. 3A). Sparse bivalve fossils are present in the grey oolitic limestone and purple marl under the microbial mounds (Fig. 3B, C, D, E). These strata are completely devoid of macrofossils in outcrop.

3. Methods

Each section was examined through field logging to produce high-resolution stratigraphic columns, specifically for microbial mounds. All microbial mound samples were extracted from hand samples for petrographic and internal fabric analyses. Ten microbial mound hand samples were slabbed and polished for macroscopic examination. More than 100 thin sections were analyzed using a Nikon LV100POL polarizing microscope. Sediments were classified according to Dunham (1962).

Twenty microbial mound samples from the 1st member of the Feixianguan Formation were prepared for micro-analysis using a scanning electron microscope (SEM). Freshly fractured pieces of microbial mound samples were prepared. All samples were cleaned in a deionized

water bath, dried, and then gold-coated for surface texture and Energy Dispersive X-ray Spectrometry (EDS) analyses using a Quanta 250 FEG at the State Key Laboratory of Oil and Gas Reservoir Geology and Exploitation, Chengdu University of Technology, China.

For further internal fabric analysis, fluorescent imaging was conducted to check the distribution of residual organic matter within the microbial mounds. This fluorescence microscopy was performed on a Leica DM4500P optical microscope, with observations induced by a Hg vapor lamp equipped with a high-performance wide band-pass filter ranging from 450 to 490 nm.

Samples for conodont recovery were dissolved in glacial acetic acid (~10 %) until completely digested, wet sieved, and dried at room temperature. A heavy sodium polytungstate liquid (2.78 g/ml) was used to separate heavy fractions from the rock residue. Conodonts were handpicked under a binocular microscope. Key conodont specimens were identified and photographed using SEM.

4. Results

4.1. Ages of microbial mounds

Ten samples were collected from the Feixianguan Formation at the BMZ-A and -B sections and three samples produced in conodonts. More than 40 conodont elements were found in the 1st member and the bottom of 2nd member of the Feixianguan Formation (Figs. 2 and 4). Samples from the microbial mound complexes of the BMZ-B section were collected, but they did not contain conodonts. Overall, five species in three key genera were identified, including *Hindeodus parvus*,

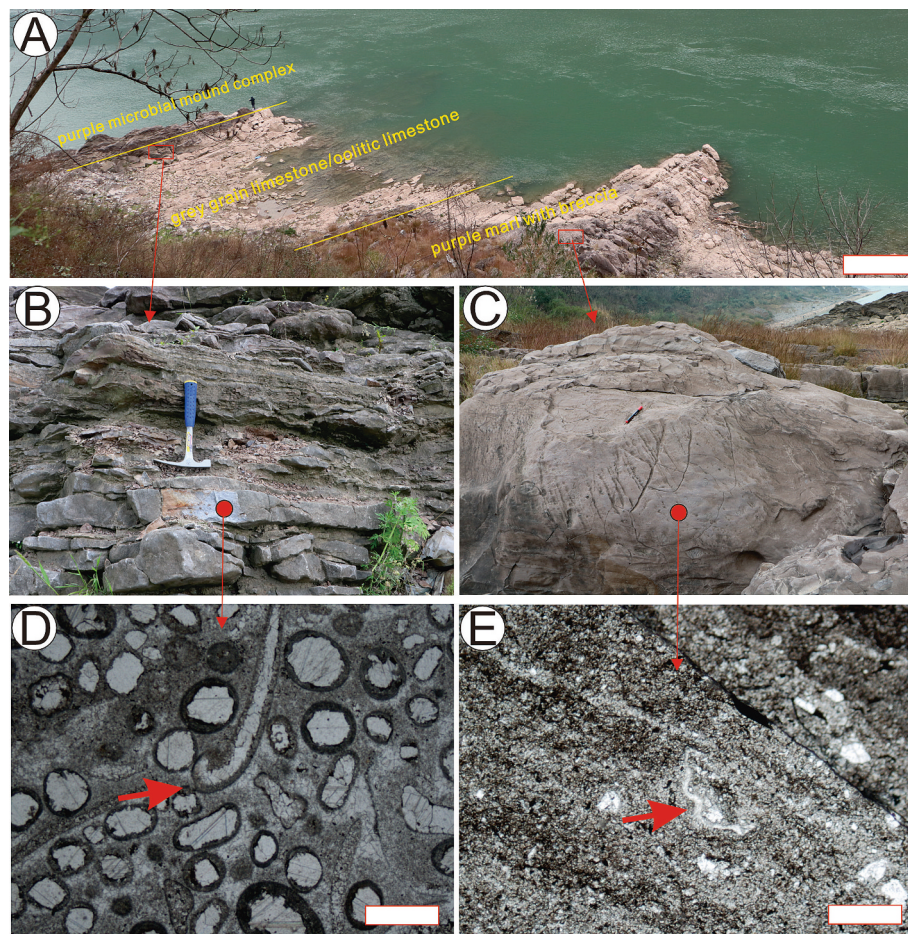


Fig. 3. The lithological stratigraphy characteristics under the microbial mound from BMZ-B section. (A) Outcrop strata characteristics under the microbial mound of 1st Member of the Feixianguan Formation at the BMZ-B section; white bar for scale measures 2 m. (B) Photograph of the grey oolitic limestone and grain limestone; the handle of the geological hammer is 15 cm. (C) Photograph of the purple marl; the marking pen is 10 cm. (D) Photomicrograph showing bivalve fossil in the oolitic limestone; white bar for scale measures 1 mm. (E) Photomicrograph showing bivalve fossil in the marl; white bar for scale measures 1 mm. (For interpretation of the references to colour in this figure legend, the reader is referred to the web version of this article.)

Hindeodus sosioensis, *Merrilina ultima*, *Isarcicella staeschei*, and *Isarcicella lobata*. One conodont zone is established from the middle 1st member to the lowest 2nd member of the Feixianguan Formation.

4.1.1. *Isarcicella staeschei* zone

The base of *Isarcicella staeschei* zone is marked by the first occurrence of *Isarcicella staeschei* and its top by the first occurrence of *Hindeodus sosioensis*. At BMZ-A, its stratigraphic range spans from 14 m to 49 m (Fig. 2), while at BMZ-B, it spans from 48 m to 82 m (Fig. 2). Associated taxa include *Hindeodus parvus*, *Merrilina ultima*, and *Isarcicella lobata*. Besides the first occurrence in sample BMZ-B-Y3, *Isarcicella staeschei* was also recognized in BMZ-B-Y4. However, the upper boundary of the zone is unclear because we did not find *Isarcicella isarcica* in the more than ten samples taken from above BMZ-B-Y3. This *I. staeschei* zone in our study may include the *I. isarcica* zone compared to others reported from elsewhere (Lai et al., 2018).

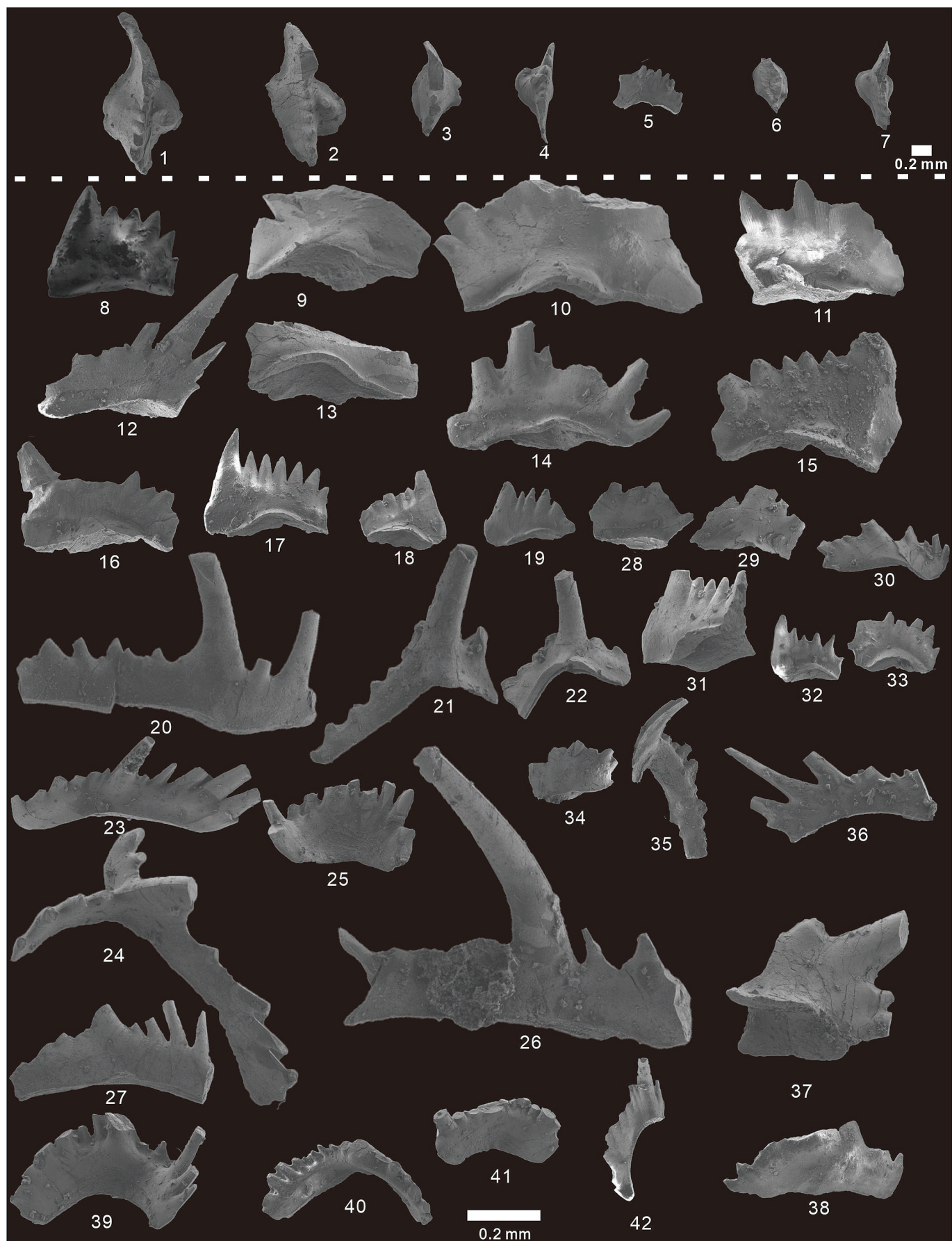
I. isarcica zone is above the *I. lobata* Zone and has been reported from South China and the Southern Alps (Perri and Farabegoli, 2003; Jiang et al., 2011; Lai et al., 2018). At BMZ-A, previous work assigned the first appearance of *I. staeschei* to a microbial mound (Duan et al., 2018), but our finding of *I. staeschei* in the middle part of the 1st member of the Feixianguan Formation moves its first occurrence about 27 m lower than before. The *I. staeschei* zone in this study corresponds to the *I. staeschei* zone at Meishan, representing the Griesbachian age (Yin et al., 2012).

4.2. Macroscopic description of microbial mounds

Prominent microbial mound complexes are found at the top of 1st member of the Feixianguan Formation (Fig. 1). These mounds are easily identified throughout the entire succession at BMZ. Lateral erosion caused by the Jiangling river exposes wide bedding surfaces, making these microbial mounds particularly noticeable due to their distinct weathering morphology. Additionally, the depositional sequence of the microbial mound complex is incompletely exposed in the TSB and YJX sections. The microbial mound complexes facies model proposed by Duan et al. (2018) comprises three distinct facies, the mound base, mound body, and mound cap (Fig. 5), all of which we can identify in our examples.

Field analysis indicates that the complete microbial mound complex is underlain by massive oolitic limestone and is capped by a red marl layer approximately 0.5 m thick (Fig. 5). In the BMZ area, the base consists of small microbial mounds (~10 cm in height) (Figs. 6C, 7C) surrounded by thin layers of marl and oolitic limestone (Fig. 6A). These layers might have inhibited the growth of the mounds and affected their preservation. While these small microbial mounds display a stromatolitic fabric (Fig. 7C), their essentially lamellar structure and the alternating layers of purple mudstone and grey microbialite are evident upon examination of the polished surface (Fig. 7D).

The microbial mound complex bodies are visible in all investigated sections and show many distinct domal microbialites (Figs. 6A; 7A; 8A, B). These domal microbialites, tens of centimeters in height and width,

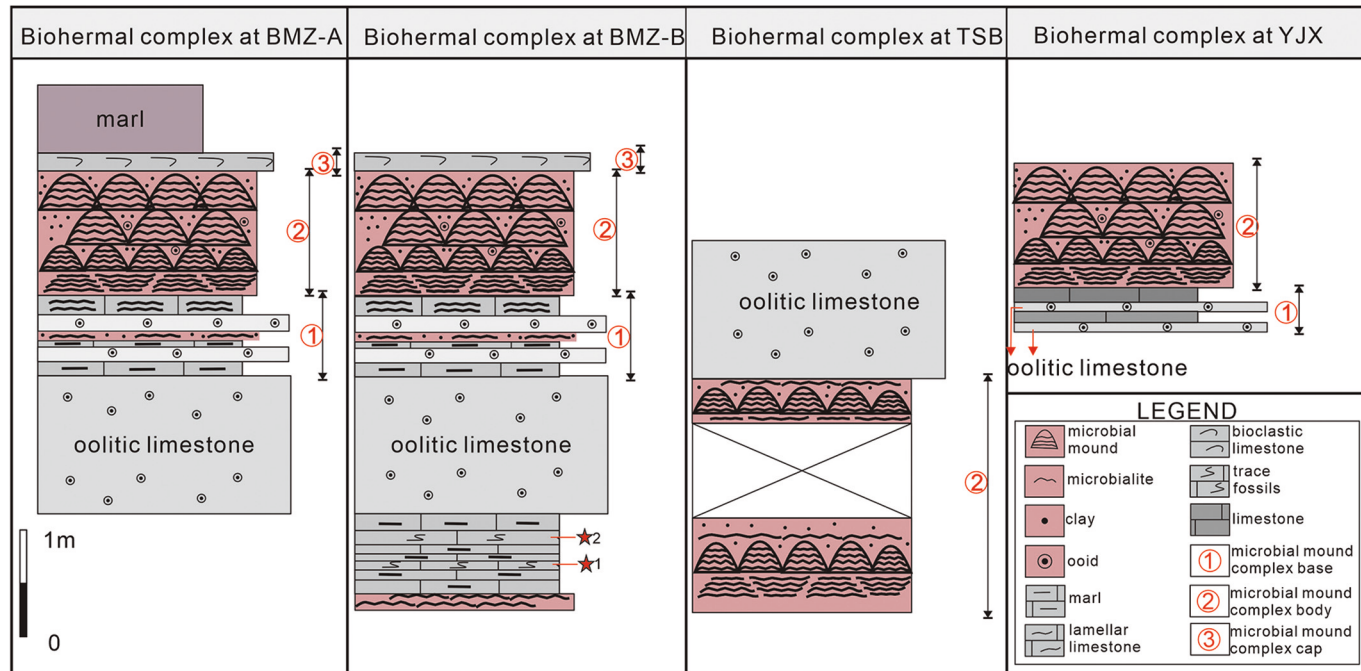


(caption on next page)

Fig. 4. SEM photos showing key conodont specimens from BMZ-A and -B sections.

- 1–2, 4. *Isarcicella staeschei*, P1 element, top view, from BMZ-B-Y3, 1st member of the Feixianguan Formation, sample 40 m of BMZ-B.
3. *Isarcicella lobata*, P1 element, top view, from BMZ-B-Y3, 1st member of the Feixianguan Formation, sample 40 m of BMZ-B.
5. *Hindeodus parvus*, P1 element, lateral view, from BMZ-B-Y3, 1st member of the Feixianguan Formation, sample 40 m of BMZ-B.
6. *Isarcicella* sp., P1 element, top view, from BMZ-B-Y3, 1st member of the Feixianguan Formation, sample 40 m of BMZ-B.
7. *Isarcicella lobata*, P1 element, top view, from BMZ-B-Y4, 1st member of the Feixianguan Formation, sample 36.5 m of BMZ-B.
- 8, 15–19, 31–33. *Hindeodus parvus*, P1 element, lateral view, from BMZ-A-Y2, 2nd member of the Feixianguan Formation, sample 49 m of BMZ-A.
- 9–10. *Hindeodus* sp., P1 element, lateral view, from BMZ-A-Y2, 2nd member of the Feixianguan Formation, sample 49 m of BMZ-A.
11. *Hindeodus sosoensis*, P1 element, lateral view, from BMZ-A-Y2, 2nd member of the Feixianguan Formation, sample 49 m of BMZ-A.
- 12, 28, 34, 37. *Merrilina ultima*, P1 element, lateral view, from BMZ-A-Y2, 2nd member of the Feixianguan Formation, sample 49 m of BMZ-A.
13. *Hindeodus* sp., P1 element, bottom view, from BMZ-A-Y2, 2nd member of the Feixianguan Formation, sample 49 m of BMZ-A.
14. *Merrilina ultima*, P2 element, lateral view, from BMZ-A-Y2, 2nd member of the Feixianguan Formation, sample 49 m of BMZ-A.
- 20, 26. *Merrilina ultima*, S4 element, lateral view, from BMZ-A-Y2, 2nd member of the Feixianguan Formation, sample 49 m of BMZ-A.
- 21–22. *Merrilina ultima*, M element, lateral view, from BMZ-A-Y2, 2nd member of the Feixianguan Formation, sample 49 m of BMZ-A.
- 23, 38. *Merrilina ultima*, S3 element, lateral view, from BMZ-A-Y2, 2nd member of the Feixianguan Formation, sample 49 m of BMZ-A.
- 24, 27, 30, 36. *Merrilina ultima*, S0 element, lateral view, from BMZ-A-Y2, 2nd member of the Feixianguan Formation, sample 49 m of BMZ-A.
- 25, 29, 39–41. *Merrilina ultima*, S1/2 element, lateral view, from BMZ-A-Y2, 2nd member of the Feixianguan Formation, sample 49 m of BMZ-A.
- 35, 42. *Hindeodus parvus*, M element, lateral view, from BMZ-A-Y2, 2nd member of the Feixianguan Formation, sample 49 m of BMZ-A.

◀

**Fig. 5.** Sedimentary sketch of the microbial mound complex from studied sections is displayed in each table.

are formed by alternating microbial mats and argillaceous sediments (Figs. 7B; 8E). Internally, the microbial mats exhibit wavy laminae microfabrics (Figs. 6C, D; 7B, E; 8C-E). The wavy laminae, mesostructural components similar to those of stromatolites, are up to a few millimeters in thickness and display variable morphologies (Figs. 6D; 7E; 8C-E). These mound erosion surfaces are affected by chemical weathering, resulting in the purple colour (Fig. 7B).

The complete microbial mound complexes are characterized by a mound cap (Fig. 5), inhabited by abundant nektonic-pelagic microfaunal assemblages (Fig. 6F). The organisms are scattered randomly within the uppermost 5 cm of the mound (Fig. 6B), and growth interruptions of the microbial mound are observed. Thus, it is suggested that the organisms in the mound cap colonized the mounds, and together with seawater conditions, determined their development.

4.3. Description of benthic community components

The microbial mound complexes contain a diverse community, including cyanobacteria, calcispheres, microconchids, sponges, brachiopods, echinoderms, gastropods, and bivalves.

4.3.1. Microbial fabric

Under the polarizing microscope, microbial structures are commonly recognizable within the microbial mound complex of every studied section distinguished by internal body recrystallization. These calcimicrobial structures typically manifest as stalk-forming filaments resembling those of contemporary cyanobacteria. Our microbial morphology analysis identified three types of calcified cyanobacteria: *Cyanonema*, *Rivulariaceae*, and *Girvanellaceae*.

Cyanonema fossils are primarily filamentous (Fig. 9A, B), consistently uniserial and unbranched. They possess a dark boundary composed of often-laminated mud. The filaments within these communities display a relatively simple, curving morphology (Fig. 9A). Filament diameters typically range from 10 to 30 µm, breakages and consequent reproduction generally limit their length to several hundred micrometers (Fig. 9A, B). Each filament usually encases a center filled with sparry calcite, some exhibiting a columnar cell fabric (Fig. 9A). Existing data on these *Cyanonema* fossils does not enable us to identify their species.

Rivulariaceae fossils are also frequently found in microbialites within the microbial mound body, mainly uniserial and unbranched, appearing as upright or flexuous filamentous tubes filled with

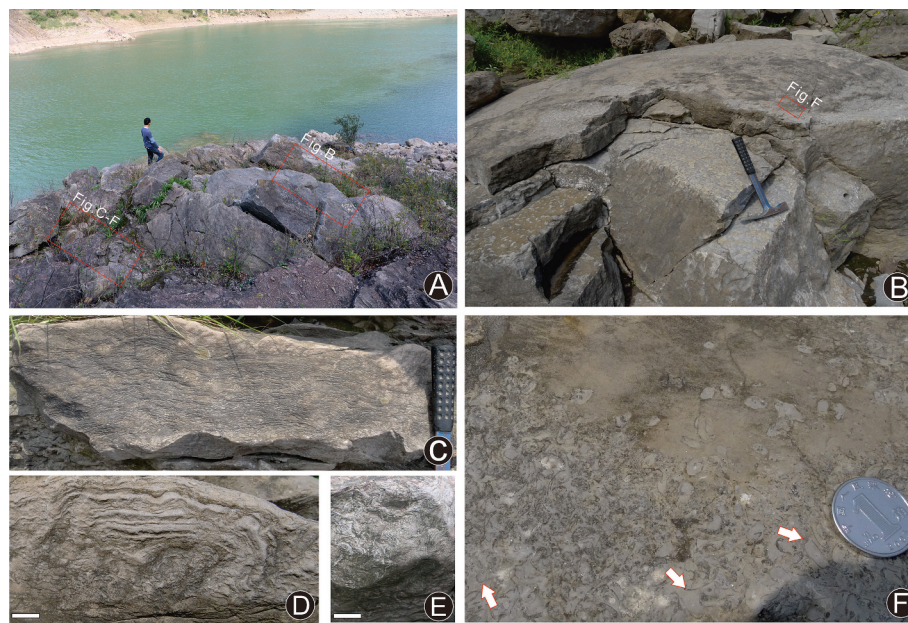


Fig. 6. Outcrop photos of the microbial mound complex from BMZ-A. (A) Overview of the microbial mound complex. (B) Field views of the mound cap; the geological hammer is 30 cm. (C) Field view of the mound body, highlighting the relatively flat lamination; the handle of the geological hammer is 15 cm. (D) Field view of the mound body with a focus on the wavy laminae; white bar for scale measures 2 cm. (E) Plan view of the mound body, showcasing the crumpled lamination; white bar for scale is 2 cm. (F) Detailed labelling from Fig. B. with arrows pointing to the abundant microfaunal presence; coin for scale is 1.9 cm.

microsparite and dark-colored sheaths (Fig. 9C, D). These sheaths can reach thicknesses of several dozen micrometers. Individual filaments commonly range from 100 to several hundred micrometers, displaying features of permineralization (Fig. 9C). In fossilized specimens, the original cell wall texture is often altered, offering limited taxonomic value. These upright filaments or pronouncedly curved tubes frequently exhibit shrinkage at their tops (Fig. 9C, D).

Girvanellaceae are regularly discerned in the microbial mound body of the TSB section, albeit subjected to intricate diagenetic alterations, and they resemble contemporary Girvanellaceae communities (Fig. 9E, F). These filaments are predominantly unbranched, with some composed of a linear sequence of recrystallized cells (Fig. 9F), and others filled with micrite (Fig. 9E). The diameter of these filamentous tubes range from 5 to 10 μm , with individual tubes approximately 100 μm in length (Fig. 9E, F). Notably, these filamentous tubes lie parallel to each other and often appear slightly curved (Fig. 9E, F).

Under a fluorescent microscope, the clotted to peloidal fabric exhibits robust fluorescence when exposed to blue excitation light (Fig. 10). The microbial mound body predominantly displays a micritic fabric, often characterized by a clotted to peloidal texture (Fig. 10C) with prevalent dark laminated layers. Some of the dark-colored laminae in the mound's upper portion are distinctly fluorescent (Fig. 10B), suggesting a residual microbial mat (Russo et al., 2000). Notably, even in the absence of well-preserved calcified bacteria, the clotted regions within the micritized texture still exhibit strong fluorescence under blue excitation light (Fig. 10D).

Observations with SEM reveal that the microbial mound typically houses calcified microbial mats and extracellular polymeric substances (EPS) (Fig. 11A-C). These mats, forming the dark laminated layers of most microbial mounds, are intricate structures. Filamentous cyanobacteria can cultivate interwoven, turf-like communities where the prevailing morphologies are meshwork and fasciculate (Fig. 11A, B). When the microbial mats retain well-preserved spherical structures, the EPS is more conspicuous (Fig. 11C), even if their surfaces tend to be fragmented. Additionally, structures resembling *Stanieria* have been observed within the microbial mound under SEM (Fig. 11D).

4.3.2. Calcareous nannofossils

Numerous calcispheres are present within the body of the microbial mound complex body, showcasing a diverse array of morphologies (Fig. 12). Observed under the SEM, the most rudimentary type radiates symmetrically from a central point (Fig. 12B-F). These calcispheres can be as large as 30 μm in diameter and manifest a spectrum of internal structures. Some have a central cavity that's either partially or fully occluded (Fig. 12B, C), while others are made up of sub-micron crystals filling the inner cavity (Fig. 12D) or contain irregular aggregates within the inner cavity (Fig. 12E). Moreover, some calcispheres are positioned so closely that their rays interpenetrate, forming compromise boundaries (Fig. 12F). When examined under an optical microscope, these calcispheres are distinguished by their distinct center, appearing as somewhat irregularly shaped calcitic grains, without rays (Fig. 12A).

4.3.3. Microconchid (coiled calcareous worm tubes)

Microconchids are small, spirally-coiled calcareous worm tubes, frequently observed in microbialites from the P-Tr boundary (Yang et al., 2011). Various morphologies of microconchids can be seen in cross-sectional views from the microbial mound complex cap (Fig. 13A-F). When examined under a polarizing microscope, microconchid tubes measure about 1 mm in length. They often display closed shapes with elliptical to kidney-like outlines, with tube diameters ranging between 100 and 200 μm (Fig. 13). The exterior of the tube is unornamented, and the shell walls are made up of laminated micritic calcite layers, each approximately a few tens of microns thick (Fig. 13B, F, G, J). Notably, the features of these shell walls are pivotal for distinguishing microconchids—with their characteristic lamellar texture—from microgastropods or spirorbid polychaetes.

4.3.4. Possible sponge fossil

In outcrop view, the microbial mound complexes consist of microbialites and marl, with sponge build-ups being rare. From thin sections of the microbialites, we identified two sponge-like fabric structures, believed to be fossil keratose sponges, which differ in their internal architecture (Fig. 14). These two categories include network fabrics (Fig. 14A, C, D) and granular single-walled fabrics (Fig. 14B), both found as discrete patches within the micrite.



Fig. 7. Outcrop photos of the microbial mound complex from BMZ-B. (A) Overview of the microbial mound complex; the geological hammer measures 30 cm in length. (B) Detailed morphology of the microbial mound body in outcrop; the lens cap is 10 cm in diameter. (C) Close-up view of the mound base, highlighting a small microbial mound; geological hammer measures 30 cm. (D) Enlargement of the red box in (C): a polished slab showing microbial mats (indicated by white arrows) and layers of argillaceous sediments (indicated by red arrows); white bar for scale measures 1 cm. (E) Detail of the wavy laminae from the mound body; the geological hammer is 30 cm. (For interpretation of the references to colour in this figure legend, the reader is referred to the web version of this article.)

The network fabrics are distinguished by their vermicular, filamentous structures, filled with straight, criss-crossing lines of sparite accompanied by nodes (Fig. 14D). These single “vermicular” or filamentous structures range from 100 to 500 µm in length and 10–50 µm in diameter. They possibly originate from the burrows or degassing/dewaterring structures of keratose sponges (Fig. 14C, D) (Neuweiler et al., 2023).

The granular single-walled fabrics, on the other hand, showcase pored calcareous chambers with micritized walls containing numerous tubular dark clots (Fig. 14B). These clotted fabrics could be a result of diagenetic alteration on sponges.

4.3.5. Other metazoan fossils

In the microbial mound complex cap, in addition to calcified cyanobacteria, there is a rich and diverse assortment of benthic invertebrates that inhabited the mound complex. The common presence of an articulate micrite constructive envelope around bioclasts in the cap suggests that microbial micritization was prevalent during the depositional stage (Fig. 15A) (Woods, 2013). Small bivalve shell fragments are the most frequently observed elements (Fig. 15C, G, H). Many of these fragments have undergone recrystallization into sparry calcite, as evident in the layered calcite patterns visible under SEM (Fig. 15C, H).

Brachiopods also feature prominently in the microbial mound complex cap, although their preservation often seems compromised by diagenetic processes (Fig. 15B). The assemblage also includes less

frequent occurrences of gastropods and echinoderm-like fossils (Fig. 15D, E, F). Gastropod fossils are typically found intact, sparry-calcite-filled, and encased by constructive micrite envelopes (Fig. 15E, F). The echinoderm-like fossil fragments exhibit a somewhat tubular appearance, are encrusted in micrite, and show characteristic network microfabrics (Fig. 15D).

5. Discussion

5.1. Marine ecosystems structures from the microbial mound complex

All community components (Fig. 16) in the microbial mound complex participated in the construction of the microbial ecosystems.

5.1.1. Primary producers in the microbial mound ecosystem

Three primary types of calcified filamentous-type cyanobacterial remains have been identified in the microbial mound complex body: *Cyanonema*, *Rivulariaceae*, and *Girvanellaceae*. These cyanobacteria exhibit considerable morphological diversity, whereas coccoid-type cyanobacterial remains are found in comparatively lower abundances in our study. Previous researchers have suggested that coccoid-type cyanobacteria, including genera like *Polybessurus*, *Microcystis*, *Staineria*, and *Gakhumella*, predominantly constitute the microbial communities of the Permian-Triassic boundary microbialites (e.g., Wu et al., 2016; Kershaw et al., 2021). Consequently, the microbial mound



Fig. 8. Outcrop photos of the microbial mound complex bodies from TSB and YJX. (A) Domal microbialites from TSB. (B) Domal microbialites from YJX. (C) Detailed morphology of the wavy laminae in domal microbialites from YJX; the coin for scale measures 2.5 cm in diameter. (D) Further detail of the wavy laminae in domal microbialites from YJX; white bar for scale is 1 cm. (E) Another detailed view of the wavy laminae in domal microbialites from YJX; the lens cap for scale is 10 cm in diameter.

complexes exhibit a distinct algal community composition when compared to other microbialites of the Permian-Triassic boundary.

Calcified filamentous-type cyanobacteria are prevalent in contemporary marine environments (Riding, 2012). Representing some of the most abundant and widespread primary producers in marine ecosystems, they play a vital role in the ecosystem's productivity (Couradeau et al., 2012). Sano and Nakashima (1997) discovered a flourish of filamentous cyanobacteria in the Griesbachian microbial bindstones of Japan. These cyanobacteria were perceived as dominant species in the shallow marine ecosystem after the mass extinction. This observation suggests that both coccoid-type and filamentous-type cyanobacteria had parallel ecological roles in microbialites during the Griesbachian. However, their adaptive strategies in response to the environment might have been distinct, with survival tactics of filamentous-type cyanobacteria diverging significantly from those of coccoid-type cyanobacteria (Pocs, 2009).

Calcified filamentous-type cyanobacteria present in the microbial mound complexes are pivotal as reef-building microorganisms. The microbial mats they form typically exhibit strong fluorescence under a fluorescent microscope, suggesting that these cyanobacteria are rich in

organic matter (Fig. 10). Such mats likely serve as a source of nutrients for primary consumers. All microbial mounds display laminar structures characterized by wavy microfabrics (Figs. 6–8) as described by Riding, (2000). These laminar structures are predominantly composed of calcified microbial mats and extracellular polymeric substance (EPS) when observed under SEM (Fig. 11). This suggests that the genesis of the microbial mound could be attributed to the proliferation of cyanobacteria. It may also be related to swift calcification and sediment-binding processes during the Griesbachian (Foster and Twitchett, 2014). A limited number of coccoid-type cyanobacteria have been found in the thin limestone layers at the base of the microbial mounds complex, but only under the SEM (Fig. 11D). These two types of cyanobacteria are probably not in a symbiotic relationship, but their mineral compositions are similar, consisting of calcium carbonate. Recent studies, such as Zhang et al. (2020), have shown that coccoid-type cyanobacteria (e.g., *Polybessurus*-like fossils) are prevalent in the Permian-Triassic boundary microbialites in South China. Both filamentous-type cyanobacteria and coccoid-type cyanobacteria were first reported in Precambrian, and are common in modern marine sediments (e.g. Schopf and Kudryavtsev, 2012). Therefore, the observed morphological variations of the

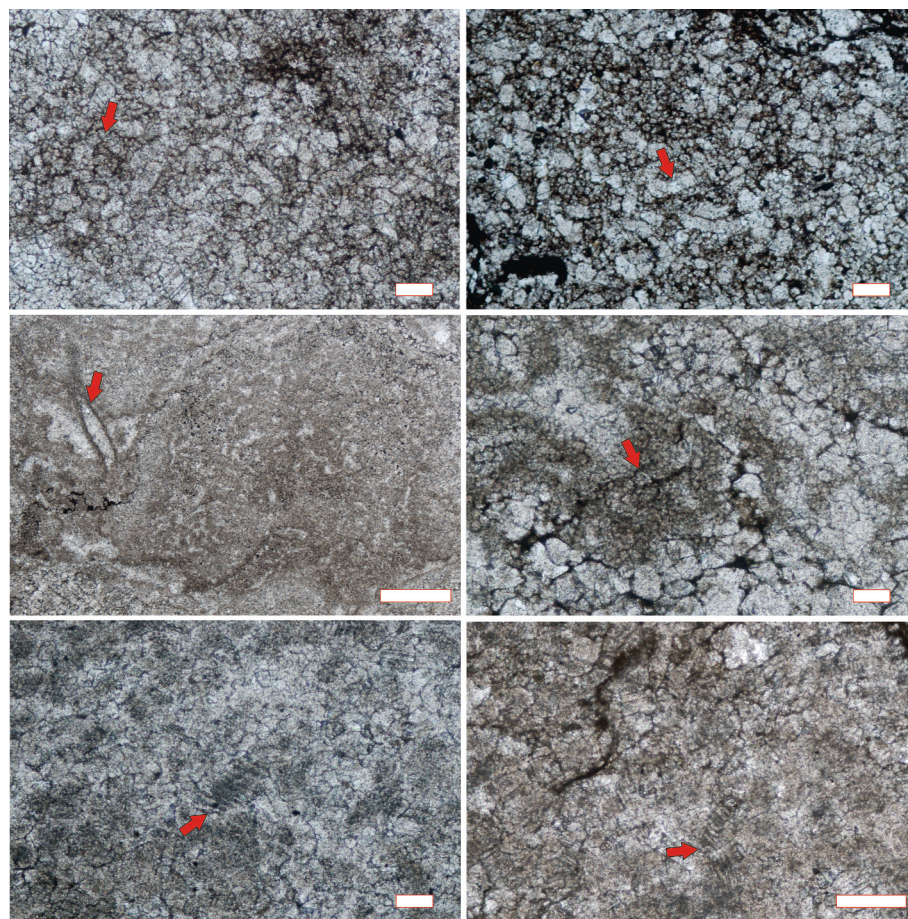


Fig. 9. Calcified cyanobacteria as observed in thin section: (A) Red arrow indicate *Cyanonema*, white bar for scale is 0.1 mm; (B) Red arrow indicate *Cyanonema*, white bar for scale is 0.1 mm; (C) Red arrow indicate *Rivulariaceae*, white bar for scale is 1 mm; (D) Red arrow indicate *Rivulariaceae*, white bar for scale is 0.1 mm; (E) Red arrow indicate *Girvanellaceae*, white bar for scale is 0.1 mm; (F) Red arrow indicate *Girvanellaceae*, white bar for scale is 0.1 mm. (For interpretation of the references to colour in this figure legend, the reader is referred to the web version of this article.)

dominant cyanobacterial taxa in microbial mounds and those in Permian-Triassic boundary microbialites are unlikely to reflect evolutionary changes. We infer that the reason for morphological differences among cyanobacteria might be due to changes in ancient marine conditions during the Griesbachian (e.g. Haas et al., 2006; Li et al., 2018; Biswas et al., 2020).

Calicispheres, abundant in the microbial mound complex, exhibit diverse morphologies under SEM examination (Fig. 12). These calcareous nannofossils were sparse during the pre-Permian (e.g., Bown et al., 2004), but began to appear in abundance sporadically during the Middle Permian (e.g., Preto et al., 2013; Dal Corso et al., 2021). Most documented Triassic calicispheres are found in Carnian (Late Triassic) layers (Bellanca et al., 1995; Preto et al., 2013). However, recent studies have identified a significant presence of calicispheres in the microbialite of the Permian-Triassic (P-Tr) boundary—specifically in the *Hindeodus parvus* zone—in the upper Yangtze (Wu et al., 2017, 2022). Intense diagenetic modifications have significantly obscured the taxonomic details of these calicispheres. Wu et al. (2022) observed that calicispheres in the P-Tr microbialite have a distinctive spiral structure in their nucleus.

Preto et al. (2013) and Dal Corso et al. (2021) suggest that the Carnian calicispheres were linked to the proliferation of planktonic calcareous microorganisms, such as dinoflagellates. This bloom, and its subsequent preservation, was likely due to biogeochemical alterations during the Carnian Pluvial Episode (CPE). Similarly, calicispheres from Cretaceous Pre-Salt lacustrine deposits of the Campos Basin originated from planktonic calcareous organisms (Chafetz et al., 2018). These

organisms floated in the water column before eventually settling at the water-sediment interface, as noted by Chafetz et al. (2018). Varejão et al. (2019) proposed that the calcispheres often found in Cretaceous microbialites are the outcome of radial aragonitic crystal precipitation around peloids. These peloids form by the amalgamation of carbonate nanoglobules enveloping decayed organic material. Hence, the formation of calicispheres can be attributed both to planktonic calcareous microorganisms and to specific environmental conditions.

5.1.2. Primary consumers in the microbial mound ecosystem

In the microbial mound ecosystem, there are potential primary consumers such as microconchids, sponges, and other invertebrates (see Figs. 13–15). Microconchids share similarities with modern calcareous worm tubes, such as spirorbid tubes, in terms of morphology and lifestyle (Yang et al., 2015). The primary organisms for making these microconchids are controversial (e.g. Fagerstrom, 1996; Taylor and Vinn, 2006). Recent micro-morphological research suggest that microconchids might have been formed by a phoronid (Yang et al., 2021). Microconchids appear in marine settings in the Late Ordovician and began colonizing continental settings during the Early Devonian (Taylor and Vinn, 2006; Zaton et al., 2012). They inhabit all climatic zones, usually living in groups and surviving by consuming suspended organic matter in the environment (Zaton et al., 2012; Yang et al., 2021); indeed, opportunistic microconchids were the first skeletonized metazoans to re-build ‘reefs’ after mass extinctions (Frasier, 2011). Most often, however, microconchids are associated with microbes forming microconchid-associated microbialites during the Permian-Triassic

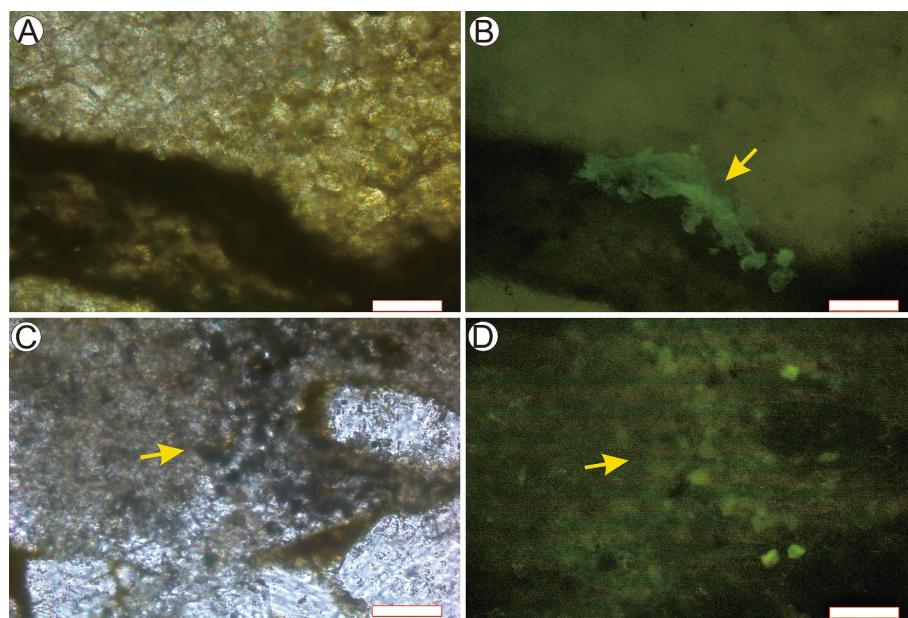


Fig. 10. Fluorescence micrographs of the microbial mound body. (A) Dark laminated layers from the upper section of the microbial mound, observed under transmissive light. (B) The same area as depicted in (A); note the fluorescence highlighting the residual microbial mat attached to the dark layers. (C) Clotted fabrics (indicated by the yellow arrow) from the lower section of the microbial mound, viewed under transmitted light. (D) The same area as shown in (C); the clotted fabrics exhibit strong fluorescence. For all images, scale bars measure 100 µm in length. (For interpretation of the references to colour in this figure legend, the reader is referred to the web version of this article.)

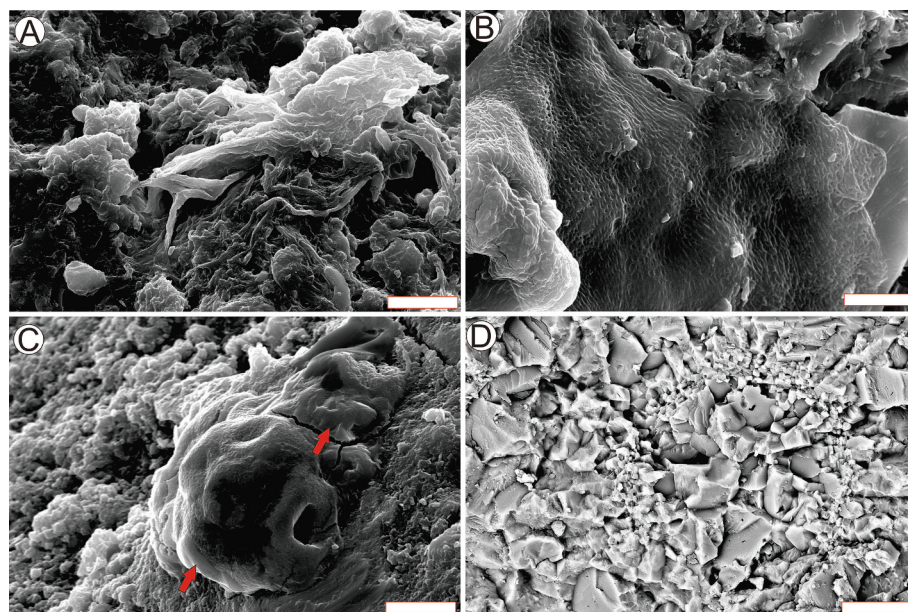


Fig. 11. SEM images of micro-fabric detected in the microbial mound. (A) Calcified microbial mats, floating turf-like communities on carbonate matrix. Scale bar is 20 µm. (B) Calcified microbial mats, scale bar is 10 µm. (C) Extracellular polymeric substances (EPS) by the red arrow, scale bar is 10 µm. (D) Putative coccoid cyanobacterial fossil, scale bar is 50 µm. (For interpretation of the references to colour in this figure legend, the reader is referred to the web version of this article.)

boundary interval (He et al., 2013; Zatoní et al., 2018; Heindel et al., 2018). In our study, the microconchids, which are oxygen-dependent invertebrates, and filamentous-type cyanobacteria lived synergistically to form the microbial mound complex body and cap during the Griesbachian. As opportunistic organisms, they were also capable of spreading rapidly and dominating the shallow marine ecosystem during the Early Triassic.

In the microbial mound body, sponges such as keratose sponges can serve as consumers and dwellers. They are often found in deep-time microbialites such as stromatolites (Friesenbichler et al., 2018; Lee

and Riding, 2021). Lee and Riding (2021) suggest that calcification of sponges in the microbialites might have been promoted by calcifying endosymbiotic bacteria. The more common types of sponges found in the microbialites examined in previous studies have been identified and demonstrated to be keratose sponges (e.g. Luo and Reitner, 2014; Lee and Riding, 2021; Wu et al., 2022). Unlike most sponges, the keratose sponges lack mineralized constituents, and have no obvious macro-form (Wörheide, 2008). In thin section, however, these fossil keratose sponges may be identified by their fibrous spongin network and absence of spicules (Neuweiler et al., 2023). Thus, the vermiform fabric and

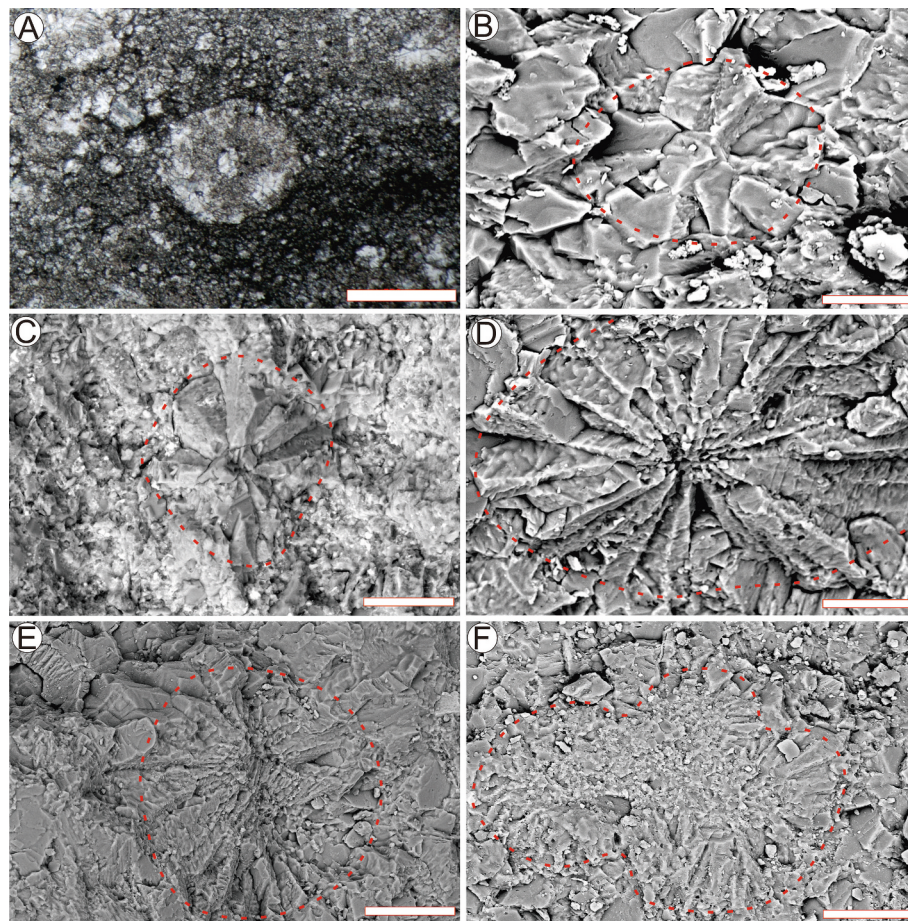


Fig. 12. Morphological variability of calcispheres in the microbial mound complex body, the red dashed line encloses calcispheres: (A) Calcispheres observed in thin sections; scale bar: 500 μm . (B) Calcisphere showcasing a centrally occluded cavity; scale bar: 20 μm . (C) Calcispheres showcasing a centrally occluded cavity with distinct rays; scale bar: 20 μm . (D) Near-spherical cluster containing submicron rhombohedral crystals in its nucleus; scale bar: 20 μm . (E) Calcisphere with an irregularly aggregated nucleus; scale bar: 50 μm . (F) Calcispheres positioned so closely that their rays form reciprocal compromise boundaries; scale bar: 25 μm . (For interpretation of the references to colour in this figure legend, the reader is referred to the web version of this article.)

fibrous spongin network (Fig. 14A, C, D) found in the microfacies of the microbial mound body were assigned to keratose sponges. Additionally, we also found other sponges in the microbial mound body, with aspicular walls with numerous tubular pores, with the most primitive forms having just a single wall (Fig. 14B). These taxonomically important features suggest that the sponges may have undergone diagenetic alteration on sponges. Overall, diverse sponges flourished together with microconchids in the microbial mound ecosystem.

5.1.3. Major fossil groups in the microbial mound cap

The communities in the microbial mound cap were dominated by benthic invertebrates (Fig. 15). Early Triassic oceans are widely characterized by low benthic oxygen levels (e.g., Grice et al., 2005); thus, oxygen produced by microbial mats may have been crucial for sustaining the mound community. The dominance switch from cyanobacteria to benthic invertebrates in microbial mound cap communities indicates that the mound cap serves as a refuge for these invertebrates, where some of them are fed and were possibly supplied with oxygen by primary producers (Foster and Twitchett, 2014; Twitchett et al., 2015). The invertebrates present in the mound cap, includ bivalves and gastropods, as well as echinoderms and microconchids. These communities are non-actualistic and anomalous in Early Triassic paleocommunities, in which they survived by opportunistic behavior (Fraiser and Bottjer, 2005). Indeed, the proliferation of benthic invertebrates in the microbial mound cap is probably due to not only the variety of environmental stresses because that the complete ecosystems had not recovered

(Kershaw et al., 2007). Some researchers suggest that the benthic invertebrates occasionally found in the microbialites are not constructors (e.g. Yang et al., 2011). However, we found that the microbial mound cap has a framework of reef metazoans (Fig. 6F), in which the fossils usually exhibits micrite constructive envelopes in thin section (Fig. 15). Thus, the microbial mound cap provides hospitable conditions for the recovery of benthic invertebrates, resulting in a degree of ecological relaxation in which metazoans could flourish while simultaneously creating a haven for development of reef structures.

5.2. An ‘oasis’ within the catastrophic ocean?

Following the EPME, the earliest Early Triassic (Griesbachian) interval is considered to have been a depressed world within marine ecosystems (McGhee Jr. et al., 2004). Although the recovery varied in time and space, benthic functional groups in marine ecosystems experienced significant loss at the global scale during the Griesbachian (Twitchett et al., 2004). During the early phase of recovery, shallow marine ecosystems were dominated by microbial communities (Chen and Benton, 2012), and the rebuilding of ecosystems was not fully achieved. Researchers have shown that relatively diverse metazoan communities have been detected in the microbialites, leading to the suggestion of a ‘microbialite refuge’ hypothesis (Forel et al., 2013). The term refuge refers to organisms that migrate during times of environmental stress from their normal habitat (Jablonski and Flessa, 1986). This earliest Triassic ‘microbialite refuge’ likely facilitated the recovery

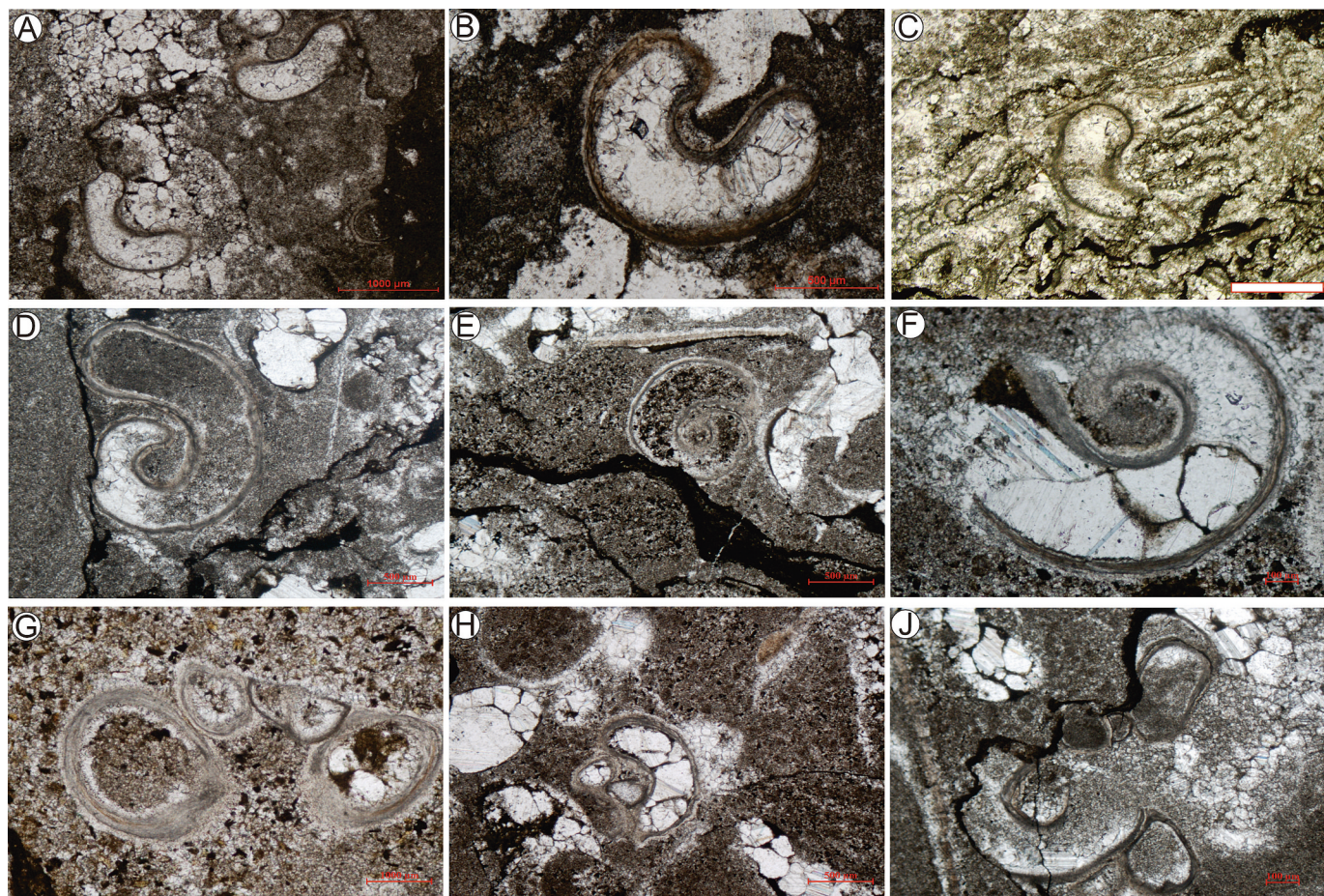


Fig. 13. Microconchids in thin sections. (A-F) Arbitrary sections of microconchids; note the internal part of the tube underwent diagenetic recrystallization. (G) Vertical sections of microconchids. (H-I) Longitudinal section of microconchids.

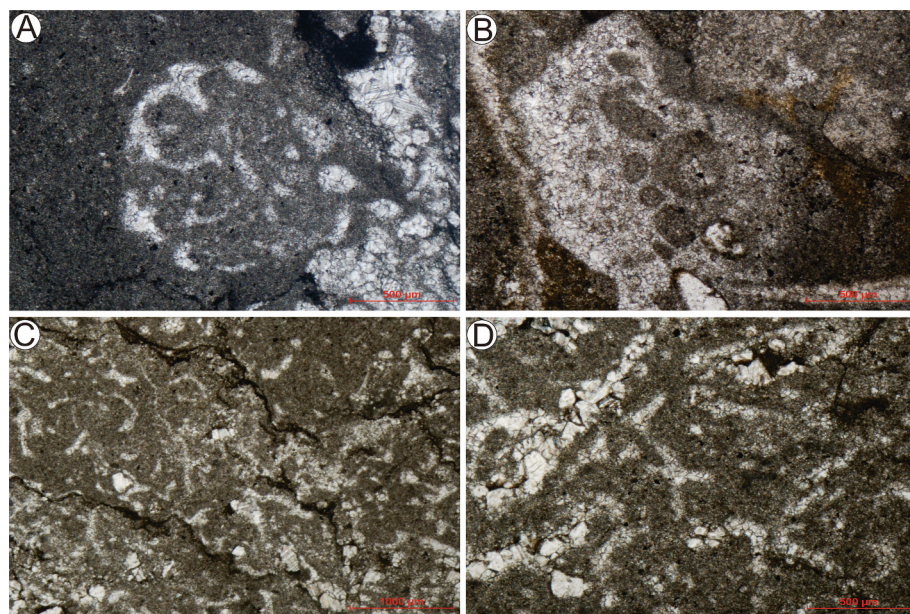


Fig. 14. Sponge-like structures observed in thin section. (A) Close-up of a demosponge-like fabric, showing the characteristic vermiform pattern. (B) Features of conical demosponge. (C) Detail of keratose sponge fabric highlighting the intricate fiber network. (D) Another view of keratose sponge fabric, with emphasis on the abrupt coarsening at the junctions.

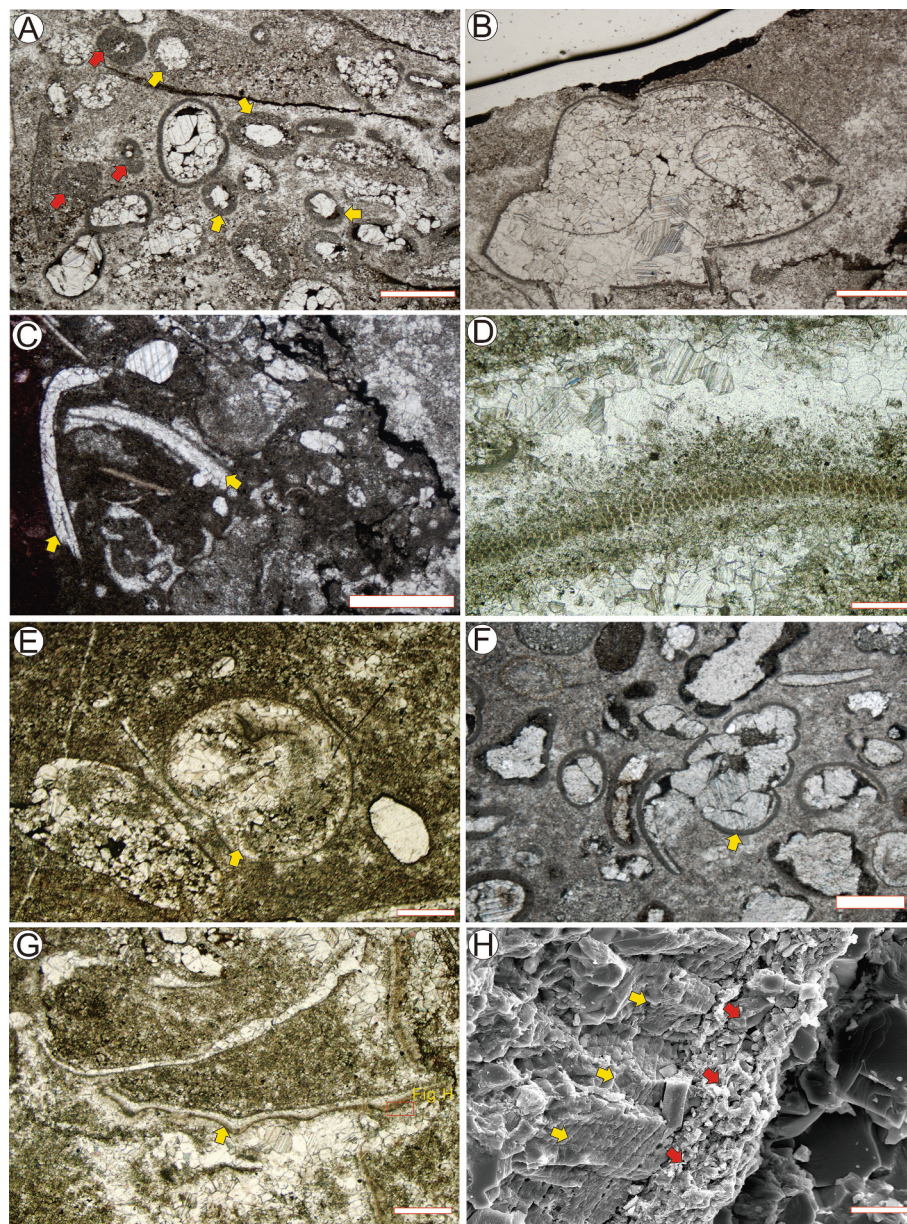


Fig. 15. Examples of benthic fauna fossils from the microbial mound complexes. (A) Micrite envelopes: fully micritized grains (red arrows) and partially micritized grains (yellow arrows); scale bar is 1000 µm. (B) Brachiopod; scale bar is 1000 µm. (C) Bivalve debris; scale bar is 1000 µm. (D) Echinoderm-like fossils; scale bar is 100 µm. (E) Transverse section of a gastropod; scale bar is 500 µm. (F) Longitudinal section of a gastropod; scale bar is 1000 µm. (G) Bivalve debris; scale bar is 500 µm. (H) Detail from (G) shown in SEM view: Shell fragments (yellow arrows) and micrite envelopes (red arrows); scale bar is 50 µm. (For interpretation of the references to colour in this figure legend, the reader is referred to the web version of this article.)

of benthic communities in the immediate aftermath of the EPME and suggests that it might also represent a taphonomic window for exceptional preservation of the biota (Forel et al., 2013; Chen et al., 2022). We suggest that the Griesbachian microbial mound has allowed for diverse fossil assemblages to be preserved during intervals of poor preservation.

Previous interpretations of early Triassic ecosystem recovery in the Yangtze region reflect the step-wise establishment of a fully functional trophic structure spanning from primary producers to top predators. Thus, benthic marine ecosystems might be in stepwise recovery in the Yangtze region with unrecorded geographic expansions during the Griesbachian. In Japan, gastropod fossils, worm tubes, and ostracod fossils were found in the basal member of Kamura Formation (Griesbachian) (Sano and Nakashima, 1997), indicating that potential meso-consumers existed in the Griesbachian marine ecosystem. Therefore, more complex marine ecosystems may have existed in the Griesbachian

despite the environmental stress. Our reconstruction of ecosystems (Fig. 17) during the earliest Triassic shows that the environmental pressures were possibly ameliorated for metazoans in the microbial mound. The metazoan communities and microbial communities presented here are therefore of first importance in understanding marine ecosystem recovery following the EPME.

There was a relatively complex marine ecosystem in the late Diererian (Dai et al., 2023), about 1 Myr after the EPME. Stepwise, the first occurrence of a diverse, complex marine ecosystem began in the early Smithian in the Nanpanjiang Basin (Song, 2011). In the Spathian, marine ecosystems were comprised of ever more diverse trace fossil assemblages, and more reef framework builders indicate that functionally complex, and trophically multilevel marine ecosystems occurred in the late Early Triassic (Kelley et al., 2023). Previous studies have shown that reef and non-reef ecosystems differ in their recovery patterns and tempo,

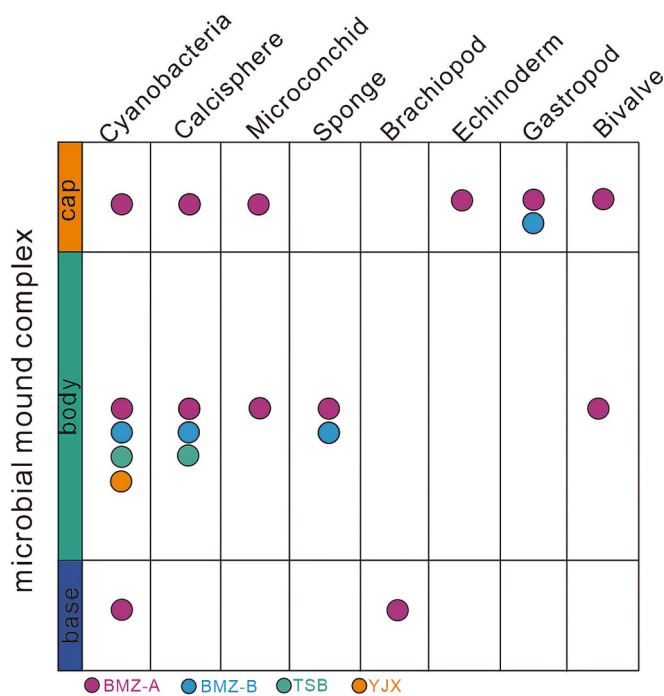


Fig. 16. Distribution of community components throughout the microbial mound complex in the study sections.

with the full recovery of metazoan-algal reefs ecosystems being slower than the non-reef ecosystems in the Early Triassic (Kelley et al., 2023).

Conodont data from this study indicate that metazoan communities in the mound complex were thriving in the Griesbachian. These metazoans are significantly different in geological chronology and biodiversity from the microbialite refuges described before (Forel et al., 2013). Although metazoans from the Griesbachian microbial mounds remain incompletely sampled, we suggest that the Early Triassic stepwise recovery model is perhaps over-simplified (Fig. 18). To some extent, the microbial mound complex is an ‘oasis’ that may have provided a livable habitat for faunas. In summary, these microbial mounds are not only the product of earliest Triassic environmental stress, but the ‘Noah’s Ark’ for survival of metazoans shortly after the EPME.

6. Conclusions

In the Chongqing area of the Yangtze block, mound structures containing microbial and metazoan fossil are present in the 1st member of Feixianguan Formation carbonate strata representing inner platform settings. The flourishing of these metazoans is strictly associated with microbial mounds and provides evidence for the existence of primary producers in the locations where they lived. They grew during the Griesbachian which is defined by the *Isarciocella staeschei* conodont zone. Although microbial mounds may have grown under the influence of dysoxic waters, the filamentous-type cyanobacteria can create a relatively oxic micro-environment for metazoans. These microbial mound complexes flourished in the Griesbachian, during which entire ecosystems had not yet been reassembled from low-diversity survivor and opportunistic metazoan assemblages. Microbial mound complexes

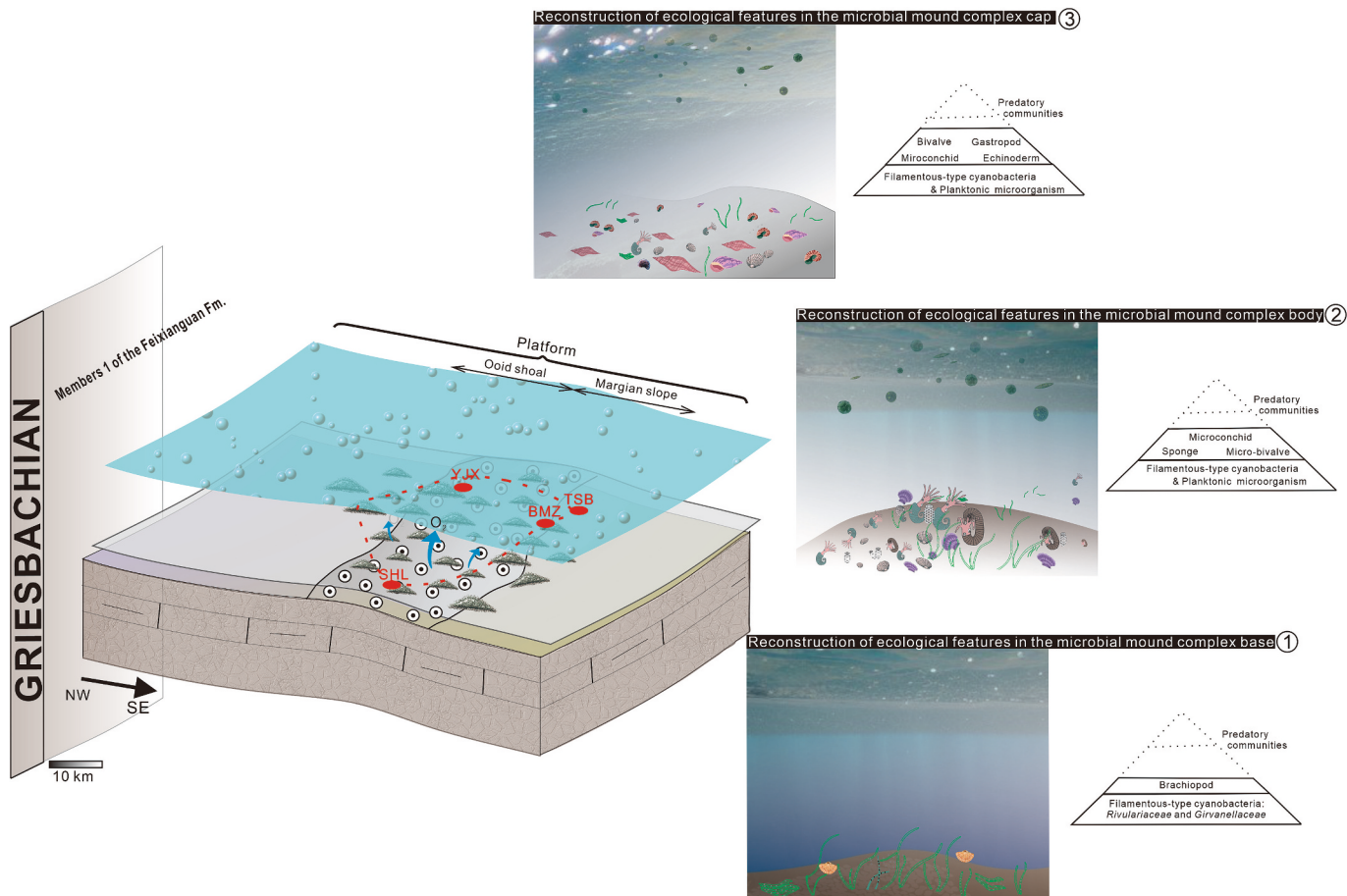


Fig. 17. Conceptual models showing the nature and distribution of the microbial mound complexes and their reconstruction of the community in the 1st member of the Feixianguan Formation.

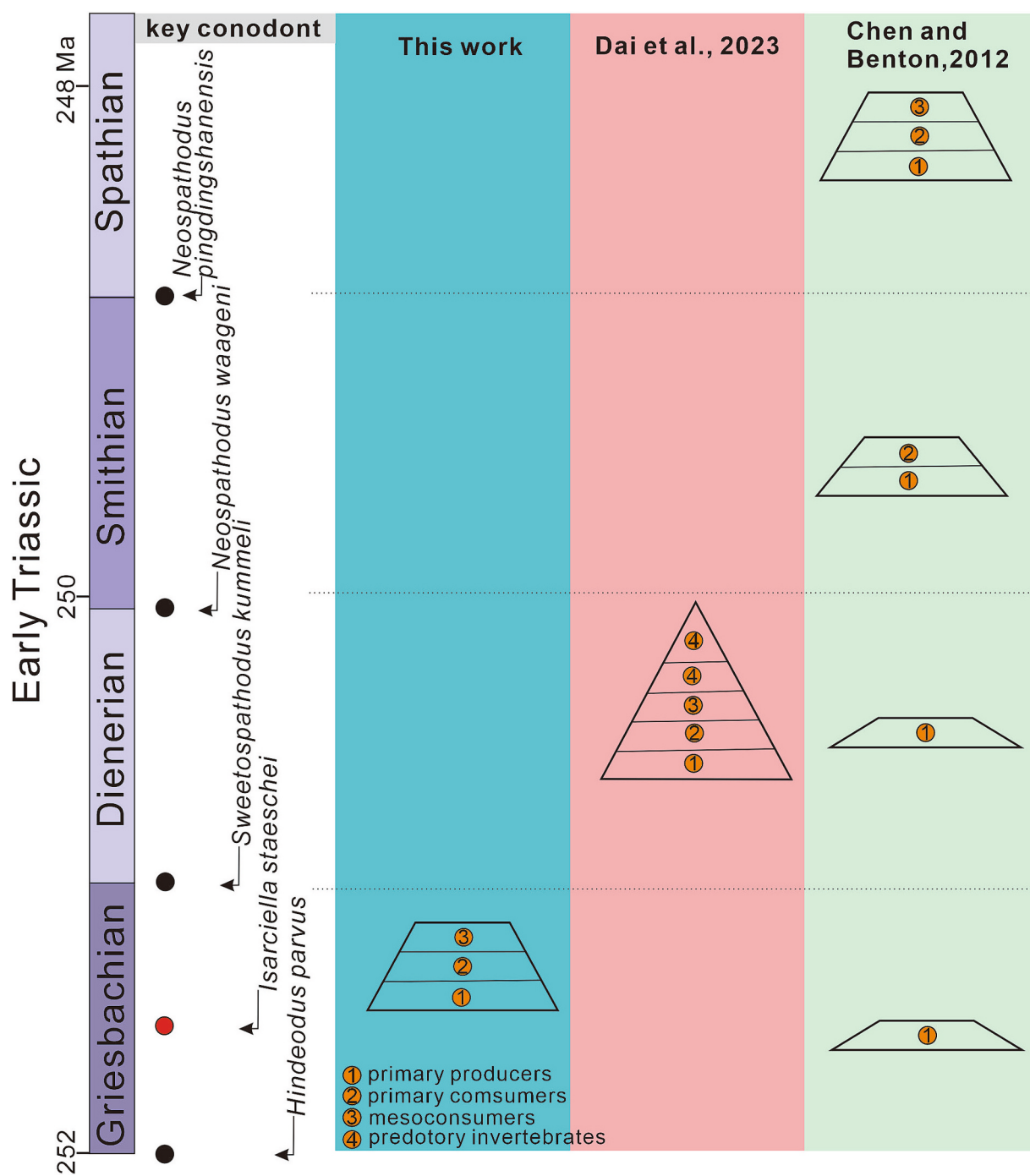


Fig. 18. Ecological features of the Griesbachian microbial mound and comparison with other main marine ecosystem (Jiang et al., 2011; Burgess et al., 2014).

add to the record about an “oasis” during the immediate aftermath of the most devastating extinction for metazoans from the inhospitable marine environments.

CRediT authorship contribution statement

Dan Qiao: Writing – review & editing, Writing – original draft, Visualization, Methodology, Investigation, Funding acquisition, Conceptualization. **Zhiqiang Shi:** Visualization, Resources, Project administration, Methodology, Investigation, Funding acquisition, Formal analysis, Data curation, Conceptualization. **Jiangong Wang:** Visualization. **Kui Wu:** Data curation. **Shenyuan Peng:** Data curation. **Michael J. Benton:** Visualization, Methodology, Formal analysis, Data

curation, Conceptualization.

Declaration of competing interest

The authors declare the following financial interests/personal relationships which may be considered as potential competing interests:

Zhiqiang Shi reports financial support was provided by Chengdu University of Technology. If there are other authors, they declare that they have no known competing financial interests or personal relationships that could have appeared to influence the work reported in this paper.

Acknowledgments

This project has received funding from the National Natural Science Foundation of China (Grant No. 41572085, No.42102011 and No.42172169) and the Department of Science and Technology of Sichuan Province, China (Grant No. 2021YJ0353). We thank X. Duan, Y. X. Du, and X. Zhang for assistance in sample processing. We also appreciate Y. S. Wu and reviewer for helpful suggestions on the manuscript.

Data availability

The authors confirm that all data necessary for supporting the scientific findings of this paper have been provided.

References

- Algeo, T.J., Chen, Z.Q., Fraiser, M.L., Twitchett, R.J., 2011. Terrestrial-marine teleconnections in the collapse and rebuilding of Early Triassic marine ecosystems. *Palaeogeogr. Palaeoclimatol. Palaeoecol.* 308, 1–11. <https://doi.org/10.1016/j.palaeo.2011.01.011>.
- Baud, A., Nakrem, H.A., Beauchamp, B., Beatty, T.W., Embry, A.F., Henderson, C.M., 2008. Lower Triassic bryozoan beds from Ellesmere Island, High Arctic, Canada. *Polar Res.* 27, 428–440. <https://doi.org/10.1111/j.1751-8369.2008.00071.x>.
- Bellanca, A., Di Stefano, P., Neri, R., 1995. Sedimentology and isotope geochemistry of Carnian deep-water marl/limestone deposits from the Sicani Mountains, Sicily: environmental implications and evidence for a planktonic source of lime mud. *Palaeogeogr. Palaeoclimatol. Palaeoecol.* 114, 111–129. [https://doi.org/10.1016/0031-0182\(95\)00077-Y](https://doi.org/10.1016/0031-0182(95)00077-Y).
- Biswas, R.K., Kaiho, K., Saito, R., Tian, L., Shi, Z.Q., 2020. Terrestrial ecosystem collapse and soil erosion before the end-Permian marine extinction: organic geochemical evidence from marine and non-marine records. *Glob. Planet. Chang.* 195, 103372. <https://doi.org/10.1016/j.gloplacha.2020.103372>.
- Bown, P.R., Lees, J.A., Young, J.R., 2004. In: Thierstein, H.R., Young, J.R. (Eds.), *Coccolithophores. Chapter 18.* Elsevier, pp. 481–508.
- Brayard, A., Bucher, H., Escarguel, G., Fluteau, F., Bourquin, S., Galfetti, T., 2006. The Early Triassic ammonoid recovery: paleoecological significance of diversity gradients. *Palaeogeogr. Palaeoclimatol. Palaeoecol.* 239, 374–395. doi. <https://doi.org/10.1016/j.palaeo.2006.02.003>.
- Brayard, A., Vennin, E., Olivier, N., Bylund, K.G., Jenks, J., Stephen, D.A., Bucher, H., Hofmann, R., Goudemand, N., Escarguel, G., 2011. Transient metazoan reefs in the aftermath of the end-Permian mass extinction. *Nat. Geosci.* 4, 693–697. <https://doi.org/10.1038/NGEO1264>.
- Burgess, S.D., Bowring, S., Shen, S.Z., 2014. High-precision timeline for Earth's most severe extinction. *Proc. Natl. Acad. Sci. USA* 111, 3316–3321. <https://doi.org/10.1073/pnas.1317692111>.
- Chafetz, H., Barth, J., Cook, M., Guo, X., Zhou, J., 2018. Origins of carbonate spherulites: implications for Brazilian Aptian pre-salt reservoir. *Sediment. Geol.* 365, 21–33. <https://doi.org/10.1016/j.sedgeo.2017.12.024>.
- Chen, Z.Q., Benton, M.J., 2012. The timing and pattern of biotic recovery following the end-Permian mass extinction. *Nat. Geosci.* 5, 375–383. <https://doi.org/10.1038/ngeo1475>.
- Chen, Z.Q., Kaiho, K., George, A.D., 2005. Early Triassic recovery of the brachiopod faunas from the end-Permian mass extinction: a global review. *Palaeogeogr. Palaeoclimatol. Palaeoecol.* 224, 270–290. <https://doi.org/10.1016/j.palaeo.2005.03.037>.
- Chen, Z.Q., Fang, Y., Wignall, P.B., Guo, Z., Wu, S., Liu, Z., Wang, R.Q., Huang, Y.G., Feng, X.Q., 2022. Microbial blooms triggered pyrite framboid enrichment and oxygen depletion in carbonate platforms immediately after the latest Permian extinction. *Geophys. Res. Lett.* 49. <https://doi.org/10.1029/2021GL096998>.
- Couradeau, E., Benzerara, K., Gérard, E., Moreira, D., Bernard, S., Brown, López-García, P., 2012. An early-branching microbialite cyanobacterium forms intracellular carbonates. *Science* 336, 459–462. <https://doi.org/10.1126/science.1216171>.
- Dai, X., Davies, J.H., Yuan, Z., Brayard, A., Ovtcharova, M., Xu, G., Liu, X.K., Smith, C.P. A., Schweitzer, C.E., Li, M.T., Perrot, M.G., Jiang, S.Y., Miao, L.Y., Cao, Y.R., Yan, J., Bai, R.Y., Wang, F.Y., Guo, W., Song, H.Y., Tian, L., Dal Corso, J., Liu, Y.T., Chu, D.L., Song, H., 2023. A Mesozoic fossil lagerstätte from 250.8 million years ago shows a modern-type marine ecosystem. *Science* 379, 567–572. <https://doi.org/10.1126/science.adf1622>.
- Dal Corso, J., Preto, N., Agnini, C., Hohn, S., Merico, A., Willems, H., Gianolla, P., 2021. Rise of calcispheres during the Carnian Pluvial Episode (Late Triassic). *Glob. Planet. Chang.* 200, 103453. <https://doi.org/10.1016/j.gloplacha.2021.103453>.
- Duan, X., Shi, Z., Chen, Y., Chen, L., Chen, B., Wang, L., Han, L., 2018. Early Triassic Griesbachian microbial mounds in the Upper Yangtze Region, Southwest China: implications for biotic recovery from the latest Permian mass extinction. *PLoS One* 13, e0201012. <https://doi.org/10.1371/journal.pone.0201012>.
- Dunham, R.J., 1962. Classification of carbonate rocks according to depositional texture. *AAPG Mem.* 1, 108–121.
- Fagerstrom, J.A., 1996. Paleozoic brachiopod symbioses: testing the limits of modern analogues in paleoecology. *Geol. Soc. Am. Bull.* 108, 1393–1403. [https://doi.org/10.1130/0016-7606\(1996\)108<1393:PBSTTL>2.3.CO;2](https://doi.org/10.1130/0016-7606(1996)108<1393:PBSTTL>2.3.CO;2).
- Forel, M.B., Crasquin, S., Kershaw, S., Collin, P.Y., 2013. In the aftermath of the end-Permian extinction: the microbialite refuge? *Terra Nova* 25, 137–143. <https://doi.org/10.1111/ter.2012.17>.
- Foster, W.J., Twitchett, R.J., 2014. Functional diversity of marine ecosystems after the Late Permian mass extinction event. *Nat. Geosci.* 7, 233–238. <https://doi.org/10.1038/NGEO2079>.
- Fraiser, M.L., 2011. Paleoecology of secondary tierers from Western Pangean tropical marine environments during the aftermath of the end-Permian mass extinction. *Palaeogeogr. Palaeoclimatol. Palaeoecol.* 308, 181–189. <https://doi.org/10.1016/j.palaeo.2010.12.002>.
- Fraiser, M.L., Bottjer, D.J., 2005. Restructuring in benthic level-bottom shallow-marine communities due to prolonged environmental stress following the end-Permian mass extinction. *C. R. Palevol.* 4, 583–591. <https://doi.org/10.1016/j.crpv.2005.02.002>.
- Friesenbichler, E., Richoz, S., Baud, A., Krystyn, L., Sahakyan, L., Vardanyan, S., Heindel, K., 2018. Sponge-microbial build-ups from the lowermost Triassic Chanakhchi section in southern Armenia: microfacies and stable carbon isotopes. *Palaeogeogr. Palaeoclimatol. Palaeoecol.* 490, 653–672. <https://doi.org/10.1016/j.palaeo.2017.11.056>.
- Grice, K., Cao, C., Love, G.D., Böttcher, M.E., Twitchett, R.J., Grosjean, E., Summons, R. E., Turgeon, S.C., Dunning, W., Jin, Y., 2005. Photic zone euxinia during the Permian-Triassic superoxic event. *Science* 310, 706–709. <https://doi.org/10.1126/science.1123073>.
- Guo, Z., Flannery-Sutherland, J.F., Benton, M.J., Chen, Z.Q., 2023. Bayesian analyses indicate bivalves did not drive the downfall of brachiopods following the Permian-Triassic mass extinction. *Nat. Commun.* 14, 5566. <https://doi.org/10.1038/s41467-023-41358-8>.
- Haas, J., Demeny, A., Hips, K., Vennemann, T.W., 2006. Carbon isotope excursions and microfacies changes in marine Permian-Triassic boundary sections in Hungary. *Palaeogeogr. Palaeoclimatol. Palaeoecol.* 237, 160–181. <https://doi.org/10.1016/j.palaeo.2005.11.017>.
- He, L., Wang, Y., Woods, A., Li, G., Yang, H., Liao, W., 2013. Calcareous tubeworms as disaster forms after the end-Permian mass extinction in South China. *Palaios* 27, 878–886. <https://doi.org/10.2307/23362144>.
- Heindel, K., Foster, W.J., Richoz, S., Birgel, D., Roden, V.J., Baud, A., Brandner, R., Krystyn, L., Mohtat, T., Kosun, E., Twitchett, R.J., Reitner, J., Peckmann, J., 2018. The formation of microbial-metazoan bioherms and biostromes following the latest Permian mass extinction. *Gondwana Res.* 61, 187–202. <https://doi.org/10.1016/j.gr.2018.05.007>.
- Jablonski, D., Flessa, K.W., 1986. The taxonomic structure of shallow water marine faunas: implications for Phanerozoic extinctions. *Am. Malacol. Bull.* 27, 43–66. <https://biostor.org/reference/143120>.
- Jiang, H., Aldridge, R.J., Lai, X., Yan, C., Sun, Y., 2010. Phylogeny of the conodont genera *Hindeodus* and *Isarcicella* across the Permian-Triassic boundary. *Lethaia* 44, 374–382. <https://doi.org/10.1111/j.1502-3931.2010.00248.x>.
- Jiang, H.S., Lai, X., Yan, C., Aldridge, R.J., Wignall, P., Sun, Y., 2011. Revised conodont zonation and conodont evolution across the Permian-Triassic boundary at the Shangsi section, Guangyuan, Sichuan, South China. *Glob. Planet. Chang.* 77, 103–115. <https://doi.org/10.1016/j.gloplacha.2011.04.003>.
- Joachimski, M.M., Lai, X., Shen, S., Jiang, H., Luo, G., Chen, B., Sun, Y., 2012. Climate warming in the latest Permian and the Permian-Triassic mass extinction. *Geology* 40, 195–198. <https://doi.org/10.1130/G32270.1>.
- Kelley, B.M., Yu, M.Y., Lehrmann, D.J., Altiner, D., Payne, J.L., 2023. Prolonged and gradual recovery of metazoan-algal reefs following the end-Permian mass extinction. *Geology* 51, 1011–1016. <https://doi.org/10.1130/G51058.1>.
- Kershaw, S., Crasquin, S., Forel, M.B., Randon, C., Collin, P.Y., Kosun, E., Baud, A., 2011. Earliest Triassic microbialites in Çırılık Dag, southern Turkey: composition, sequences and controls on formation. *Sedimentology* 58, 739–755. <https://doi.org/10.1111/j.1365-3091.2010.01181.x>.
- Kershaw, S., Li, Y., Crasquin-Soleau, S., Feng, Q., Mu, X., Collin, P.Y., Reynolds, A., Guo, L., 2007. Earliest Triassic microbialites in the South China block and other areas: controls on their growth and distribution. *Facies* 53, 409–425. <https://doi.org/10.1007/s10347-007-0105-5>.
- Kershaw, S., Zhang, T., Li, Y., 2021. *Calcilobes wangshenghaii* n. gen., n. sp., microbial constructor of Permian-Triassic boundary microbialites of South China, and its place in microbialite classification. *Facies* 67, 28. <https://doi.org/10.1007/s10347-021-00636-x>.
- Lai, X., Jiang, H., Wignall, P.B., 2018. A review of the Late Permian-Early Triassic conodont record and its significance for the end-Permian mass extinction. *Rev. Micropaleontol.* 61, 155–164. <https://doi.org/10.1016/j.revmic.2018.10.002>.
- Lee, J.H., Riding, R., 2021. Keratolite-stromatolite consortia mimic domical and branched columnar stromatolites. *Palaeogeogr. Palaeoclimatol. Palaeoecol.* 571, 110288. <https://doi.org/10.1016/j.palaeo.2021.110288>.
- Li, F., Gong, Q.L., Burne, R.V., Tang, H., Su, C.P., Zeng, K., Zhang, Y.F., Tan, X.C., 2018. Ooid factories operating under hothouse conditions in the earliest Triassic of South China. *Glob. Planet. Chang.* 172, 336–354. <https://doi.org/10.1016/j.gloplacha.2018.10.012>.
- Luo, C., Reitner, J., 2014. First report of fossil “keratose” demosponges in Phanerozoic carbonates: preservation and 3-D reconstruction. *Naturwissenschaften* 101, 467–477. <https://doi.org/10.1007/s00114-014-1176-0>.
- Mata, S.A., Bottjer, D.J., 2012. Microbes and mass extinctions: paleoenvironmental distribution of microbialites during times of biotic crisis. *Geobiology* 10, 3–24. <https://doi.org/10.1111/j.1472-4669.2011.00305.x>.

- McGhee Jr., G.R., Sheehan, P.M., Bottjer, D.J., Droser, M.L., 2004. Ecological ranking of Phanerozoic biodiversity crises: ecological and taxonomic severities are decoupled. *Palaeogeogr. Palaeoclimatol. Palaeoecol.* 211, 287–289. <https://doi.org/10.1016/j.palaeo.2004.05.010>.
- Neuweiler, F., Kershaw, S., Boulvain, F., Matysik, M., Sendino, C., McMenamin, M., Munnecke, A., 2023. Keratose sponges in ancient carbonates—a problem of interpretation. *Sedimentology* 70, 927–969. <https://doi.org/10.1111/sed.13059>.
- Perri, M.C., Farabegoli, E., 2003. Conodonts across the Permian-Triassic boundary in the Southern Alps. *Cour. Forschungsinst. Senck.* 245, 281–313.
- Pisera, A., 1996. Miocene reefs of the Paratethys: a review. *SEPM Concepts Sediment. Paleontol* 5, 97–104. <https://doi.org/10.2110/csp.96.01.0097>.
- Pocs, T., 2009. Cyanobacterial crust types, as strategies for survival in extreme habitats. *Acta Bot. Hungar.* 51, 147–178. <https://doi.org/10.1556/ABot.51.2009.1-2.16>.
- Preto, N., Willems, H., Guiaumi, C., Westphal, H., 2013. Onset of significant pelagic carbonate accumulation after the Carnian Pluvial Event (CPE) in the western Tethys. *Facies* 59, 891–914. <https://doi.org/10.1007/s10347-012-0338-9>.
- Pruss, S.B., Bottjer, D.J., 2004. Late Early Triassic microbial reefs of the western United States: a description and model for their deposition in the aftermath of the end-Permian mass extinction. *Palaeogeogr. Palaeoclimatol. Palaeoecol.* 211, 127–137. <https://doi.org/10.1016/j.palaeo.2004.05.002>.
- Qiao, Z.F., Li, G.R., Long, S.X., Jiang, Z.Z., Hu, W.Y., Li, W.M., 2010. Characteristics and evolution model of sequence stratigraphy of Feixianguan Formation in the northeast of Sichuan Basin (in Chinese with English abstract). *Acta Sedimentol. Sin.* 28, 462–470. <https://doi.org/10.14027/j.cnki.cjxb.2010.03.025>.
- Qiao, Z.F., Janson, X., Shen, A., Zheng, J., Zeng, H., Wang, X., 2016. Lithofacies, architecture, and reservoir heterogeneity of tidal-dominated platform marginal oolitic shoal: an analogue of oolitic reservoirs of Lower Triassic Feixianguan Formation, Sichuan Basin, SW China. *Mar. Pet. Geol.* 76, 290–309. <https://doi.org/10.1016/j.marpetgeo.2016.05.030>.
- Riding, R., 2000. Microbial carbonates: the geological record of calcified bacterial-algal mats and biofilms. *Sedimentology* 47, 179–214. <https://doi.org/10.1046/j.1365-3091.2000.00003.x>.
- Riding, R., 2012. A hard life for cyanobacteria. *science* 336, 427–428. <https://doi.org/10.1126/science.124126>.
- Russo, F., Mastandrea, A., Stefani, M., Neri, C., 2000. Carbonate facies dominated by syndepositional cements: a key component of Middle Triassic platforms. The Marmolada case history (Dolomites, Italy). *Facies* 42, 211–226. <https://doi.org/10.1007/BF02562573>.
- Sano, H., Nakashima, K., 1997. Lowermost Triassic (Griesbachian) microbial bindstone-cementstone facies, Southwest Japan. *Facies* 36, 1–24. <https://doi.org/10.1007/BF02536874>.
- Schopf, J.W., Kudryavtsev, A.B., 2012. Biogenicity of Earth's earliest fossils: a resolution of the controversy. *Gondwana Res.* 22, 761–771. <https://doi.org/10.1016/j.gr.2012.07.003>.
- Song, H.J., 2011. Recovery tempo and pattern of marine ecosystems after the end-Permian mass extinction. *Geology* 39, 739–742. <https://doi.org/10.1130/G32191.1>.
- Sun, Y.D., Joachimski, M.M., Wignall, P.B., Yan, C., Chen, Y., Jiang, H., Wang, L.N., Lai, X.L., 2012. Lethally hot temperatures during the Early Triassic greenhouse. *Science* 338, 366–370. <https://doi.org/10.1126/science.1224126>.
- Tang, H., Kershaw, S., Liu, H., Tan, X., Li, F., Hu, G., Huang, C., Wang, L., Lian, C., Li, L., Yang, X., 2017. Permian-Triassic boundary microbialites (PTBMs) in southwest China: implications for paleoenvironment reconstruction. *Facies* 63, 2–24. <https://doi.org/10.1007/s10347-016-0482-8>.
- Taylor, P.D., Vinn, O., 2006. Convergent morphology in small spiral worm tubes ('Spirorbis') and its palaeoenvironmental implications[J]. *J. Geol. Soc.* 163, 225–228.
- Twittchett, R.J., Foster, W.J., Morten, S.D., 2015. Surviving the Permian-Triassic mass extinction: the importance of respiration and body size. *Palaeontology* 58, 687–700. <https://doi.org/10.1111/pala.12168>.
- Twittchett, R.J., Krystyn, L., Baud, L., Wheeley, J.R., Richoz, S., 2004. Rapid marine recovery after the end-Permian mass-extinction event in the absence of marine anoxia. *Geology* 32, 805–808. <https://doi.org/10.1130/G20585.1>.
- Varejão, F.G., Fuersich, F.T., Warren, L.V., Matos, S.A., Rodrigues, M.G., Assine, M.L., Sales, A.M.F., Simões, M.G., 2019. Microbialite fields developed in a protected rocky coastline: the shallow carbonate ramp of the Aptian Romualdo Formation (Araripe Basin, NE Brazil). *Sediment. Geol.* 389, 103–120. <https://doi.org/10.1016/j.sedgeo.2019.06.003>.
- Wang, G.W., Li, P.P., Hao, F., Zou, H.Y., Yu, X.Y., 2015. Origin of dolomite in the third member of Feixianguan Formation (Lower Triassic) in the Jiannan area, Sichuan Basin, China. *Mar. Pet. Geol.* 63, 127–141. <https://doi.org/10.1016/j.marpetgeo.2015.01.019>.
- Wignall, P.B., Twittchett, R.J., 2002. Extent, duration, and nature of the Permian-Triassic superanoxic event. *Geological Society of America Special Papers* 365, 395–431. <https://doi.org/10.1130/0-8137-2356-6.395>.
- Woods, A.D., 2013. Microbial ooids and cortoids from the Lower Triassic (Spathian) Virgin Limestone, Nevada, USA: evidence for an Early Triassic microbial bloom in shallow depositional environments. *Glob. Planet. Chang.* 105, 91–101. <https://doi.org/10.1016/j.gloplacha.2012.07.011>.
- Woods, A.D., 2014. Assessing Early Triassic paleoceanographic conditions via unusual sedimentary fabrics and features. *Earth-Sci. Rev.* 137, 6–18. <https://doi.org/10.1016/j.earscirev.2013.08.015>.
- Wörheide, G., 2008. A hypercalcified sponge with soft relatives: vaseletia is a keratose demosponge. *Mol. Phylogenet. Evol.* 47, 433–438. <https://doi.org/10.1016/j.molphy.2008.01.021>.
- Wu, H., He, W., Shi, G.R., Zhang, K., Yang, T., Zhang, Y., Xiao, Y., Chen, B., Wu, S., 2018. A new Permian-Triassic boundary brachiopod fauna from the Xinmin section, southwestern Guizhou, south China and its extinction patterns. *Alcheringa* 42, 339–372. <https://doi.org/10.1080/03115518.2018.1462400>.
- Wu, Y.S., Yu, G.L., Jiang, H.X., Liu, L.J., Zhao, R., 2016. Role and lifestyle of calcified cyanobacteria (*Stanieria*) in Permian-Triassic boundary microbialites. *Palaeogeogr. Palaeoclimatol. Palaeoecol.* 448, 39–47. <https://doi.org/10.1016/j.palaeo.2015.11.019>.
- Wu, S., Chen, Z.Q., Fang, Y., Pei, Y., Yang, H., Ogg, J., 2017. A Permian-Triassic boundary microbialite deposit from the eastern Yangtze Platform (Jiangxi Province, South China): geobiologic features, ecosystem composition and redox conditions. *Palaeogeogr. Palaeoclimatol. Palaeoecol.* 486, 58–73. <https://doi.org/10.1016/j.palaeo.2017.05.015>.
- Wu, S.Q., Chen, Z.Q., Su, C., Fang, Y., Yang, H., 2022. Keratose sponge fabrics from the lowermost Triassic microbialites in South China: geobiologic features and Phanerozoic evolution. *Glob. Planet. Chang.* 211, 103787. <https://doi.org/10.1016/j.gloplacha.2022.103787>.
- Xie, S., Algeo, T.J., Zhou, W., Ruan, X., Luo, G., Huang, J., Yan, J., 2017. Contrasting microbial community changes during mass extinctions at the Middle/Late Permian and Permian/Triassic boundaries. *Earth Planet. Sci. Lett.* 460, 180–191. doi. <https://doi.org/10.1016/j.epsl.2016.12.015>.
- Yang, H., Chen, Z.Q., Su, C., Fang, Y., Yang, H., 2011. Small microbialites from the Triassic mudstone (Tieshikou, Jiangxi, South China): geobiologic features, biogenicity, and paleoenvironmental implications. *Palaeogeogr. Palaeoclimatol. Palaeoecol.* 519, 221–235. <https://doi.org/10.1016/j.palaeo.2018.06.030>.
- Yang, H., Chen, Z.Q., Ou, W., 2015. Microconchids from microbialites near the Permian-Triassic boundary in the Zuodong Section, Baise area, Guangxi Zhuang Autonomous Region, South China and their paleoenvironmental implications. *J. Earth Sci.* 26, 157–165. <https://doi.org/10.1007/s12583-015-0554-7>.
- Yang, H., Chen, Z.Q., Wang, Y., Tong, J., Song, H., Chen, J., 2011. Composition and structure of microbialite ecosystems following the end-Permian mass extinction in South China. *Palaeogeogr. Palaeoclimatol. Palaeoecol.* 308, 111–128. <https://doi.org/10.1016/j.palaeo.2010.05.029>.
- Yin, H.F., Xie, S.C., Luo, G.M., Algeo, T.J., Zhang, K.X., 2012. Two episodes of environmental change at the Permian-Triassic boundary of the GSSP section Meishan. *Earth Sci. Rev.* 115, 163–172. <https://doi.org/10.1016/j.earscirev.2012.08.006>.
- Zatoń, M., Niedźwiedzki, G., Rakociński, M., Blom, H., Kear, B.P., 2018. Earliest Triassic metazoan bioconstructions from East Greenland reveal a pioneering benthic community in the immediate aftermath of the end-Permian mass extinction. *Glob. Planet. Chang.* 167, 87–98. <https://doi.org/10.1016/j.gloplacha.2018.05.009>.
- Zatoń, M., Vinn, O., Tomescu, A.M., 2012. Invasion of freshwater and variable marginal marine habitats by microconchid tubeworms—an evolutionary perspective. *Geobios* 45, 603–610. <https://doi.org/10.1016/j.geobios.2011.12.003>.
- Zhang, T.S., Chen, X.H., Liu, Z.C., 2012. Seismites and their geological significance in early Triassic of Southeast Sichuan basin (in Chinese with English abstract). *Acta Sedimentol. Sin.* 30, 477–489.
- Zheng, Z.Y., Zuo, Y.H., Wen, H.G., Li, D.M., Luo, Y., Zhang, J.Z., Yang, M.H., Zeng, J.C., 2023. Natural gas characteristics and gas-source comparisons of the lower Triassic Feixianguan formation, Eastern Sichuan basin. *Pet. Sci.* 20, 1458–1470. <https://doi.org/10.1016/j.petsci.2023.02.005>.
- Zhang, X.Y., Zheng, Q.F., Li, Y., Yang, H.Q., Zhang, H., Wang, W.Q., Shen, S.Z., 2020. *Polybessurus*-like fossils as key contributors to Permian-Triassic boundary microbialites in South China. *Palaeogeogr. Palaeoclimatol. Palaeoecol.* 552, 10977. <https://doi.org/10.1016/j.palaeo.2020.109770>.